AD-A095 565 TETRA TECH INC PASADENA CA F/G 20/4
STUDY ON A CAVITATING HYDROFOIL HAVING A PRACTICAL BLADE PROFIL--ETC(U)
OCT 80 O FURUYA, S MAEKAWA N00014-79-C-0234
UNCLASSIFIED TETRAT-TC-3284-03 NL

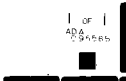

END
DATE FILMED
3-81
DTIC

Report No. TC-3284-03
Contract No. N00014-79-C-0234 P0000 1

LEVEL II

STUDY ON A CAVITATING HYDROFOIL HAVING A PRACTICAL BLADE PROFILE SHAPE

by

OKITSUGU FURUYA
SHIN MAEKAWA

TETRA TECH, INC.
630 NORTH ROSEMEAD BOULEVARD
PASADENA, CALIFORNIA 91107

OCTOBER 1980

Prepared for

DAVID W. TAYLOR NAVAL SHIP R&D CENTER
BETHESDA, MARYLAND 20084

OFFICE OF NAVAL RESEARCH
800 NORTH QUINCY STREET
ARLINGTON, VIRGINIA 22217

Approved for public release;
distribution unlimited

TETRA TECH

Report No. TC-3284-03
Contract No. N00014-79-C-0234 P0000 1

STUDY ON A CAVITATING HYDROFOIL HAVING A PRACTICAL BLADE PROFILE SHAPE

by

OKITSUGU FURUYA
SHIN MAEKAWA

TETRA TECH, INC.
630 NORTH ROSEMEAD BOULEVARD
PASADENA, CALIFORNIA 91107

OCTOBER 1980

Prepared for

DAVID W. TAYLOR NAVAL SHIP R&D CENTER
BETHESDA, MARYLAND 20084

OFFICE OF NAVAL RESEARCH
800 NORTH QUINCY STREET
ARLINGTON, VIRGINIA 22217

UNCLASSIFIED

SECURITY CLASSIFICATION OF THIS PAGE (When Data Entered)

TETRAT- REPORT DOCUMENTATION PAGE		READ INSTRUCTIONS BEFORE COMPLETING FORM
1. REPORT NUMBER TC-3284-03	2. GOVT ACCESSION NO. AD-A095 565	3. RECIPIENT'S CATALOG NUMBER
4. TITLE (and Subtitle) STUDY ON A CAVITATING HYDROFOIL HAVING A PRACTICAL BLADE PROFILE SHAPE		5. TYPE OF REPORT & PERIOD COVERED Technical - Theory & Experiment February 15, 1980-Oct. 31, 1980 6. PERFORMING ORG. REPORT NUMBER TC 3284-03
7. AUTHOR(s) Okitsugu Furuya Shin Maekawa		8. CONTRACT OR GRANT NUMBER(s) N00014-79-C-0234 P0000 1
9. PERFORMING ORGANIZATION NAME AND ADDRESS TETRA TECH, INC. 630 North Rosemead Boulevard Pasadena, CA 91107		10. PROGRAM ELEMENT, PROJECT, TASK AREA & WORK UNIT NUMBERS DWTNSR&DC (1505) Reg. 0181967/10-1-79
11. CONTROLLING OFFICE NAME AND ADDRESS David W. Taylor Naval Ship R&D Center Department of the Navy Bethesda, MD 20084		12. REPORT DATE October 31, 1980 13. NUMBER OF PAGES 81
14. MONITORING AGENCY NAME & ADDRESS(if different from Controlling Office) Office of Naval Research 800 North Quincy Street Arlington, VA 22217		15. SECURITY CLASS. (of this report) Unclassified 15a. DECLASSIFICATION/DOWNGRADING SCHEDULE

16. DISTRIBUTION STATEMENT (of this Report)

Approved for public release; distribution unlimited

17. DISTRIBUTION STATEMENT (of the abstract entered in Block 20, if different from Report)

18. SUPPLEMENTARY NOTES

Sponsored by the Naval Sea Systems Command General Hydrodynamic Research Program and administered by the David W. Taylor Naval Ship R&D Center, Code 1505, Bethesda, Maryland 20084.

19. KEY WORDS (Continue on reverse side if necessary and identify by block number)

cavitating foil
experiment
theory
partially cavitating flow
supercavitating flow

20. ABSTRACT (Continue on reverse side if necessary and identify by block number)

Experiments were conducted at the High Speed Water Tunnel of the California Institute of Technology for measuring the flow characteristics of a single foil over a full range of cavitation numbers. The blade profile shape used is that of a modified Tulin two-term camber with a blunt trailing edge. This profile shape was taken after the cross-section profile of a supercavitating propeller designed for an actual high speed hydrofoil boat. It was discovered in the experiments that the flow pattern totally changed at about an incidence angle of 2 degrees. For higher incidence angles than 2 degrees, the cavity sprang from the leading edge as was

DD FORM 1 JAN 73 1473 EDITION OF 1 NOV 65 IS OBSOLETE S/N 0102-014-6601 | 405 246

UNCLASSIFIED

SECURITY CLASSIFICATION OF THIS PAGE (When Data Entered)

expected, whereas for lower incidence angles the base cavity and sometimes double cavities appeared. The trends of the force coefficients for these different cavity-flow patterns were, of course, found to be totally different. This fact, which was never considered in the design procedure nor in the off-design prediction theory, might have caused an erroneous prediction for the thrust coefficient and efficiency of this supercavitating propeller.

In order to make comparisons with the experimental data, three new nonlinear cavity flow theories have been developed, one for the supercavitating (S/C) regime and two for the partially cavitating (P/C) regime. The results of these theories compared favorably with the experimental data, but the accuracy degraded as the cavity length became close to the chord length both in S/C and P/C ranges. The success of the present experiments has allowed us to design dummy blades for the cascade experiments to be conducted in the following phase of the present work for FY 1981.

TABLE OF CONTENTS

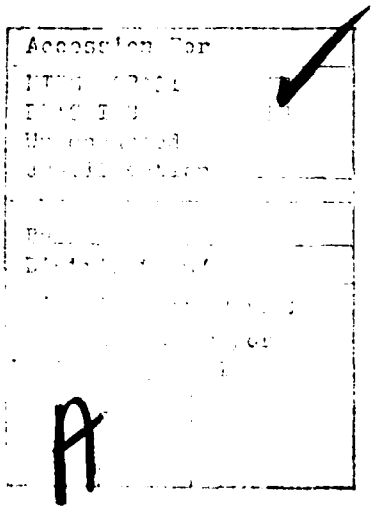

LIST OF TABLE AND FIGURES

ABSTRACT

Experiments were conducted at the High Speed Water Tunnel of the California Institute of Technology for measuring the flow characteristics of a single foil over a full range of cavitation numbers. The blade profile shape used is that of a modified Tulin two-term camber with a blunt trailing edge. This profile shape was taken after the cross-section profile of a supercavitating propeller designed for an actual high speed hydrofoil boat. It was discovered in the experiments that the flow pattern totally changed at about an incidence angle of 2 degrees. For higher incidence angles than 2 degrees, the cavity sprang from the leading edge as was expected, whereas for lower incidence angles the base cavity and sometimes double cavities appeared. The trends of the force coefficients for these different cavity-flow patterns were, of course, found to be totally different. This fact, which was never considered in the design procedure nor in the off-design prediction theory, might have caused an erroneous prediction for the thrust coefficient and efficiency of this supercavitating propeller.

In order to make comparisons with the experimental data, three new nonlinear cavity flow theories have been developed, one for the supercavitating (S/C) regime and two for the partially cavitating (P/C) regime. The results of these theories compared favorably with the experimental data, but the accuracy degraded as the cavity length became close to the chord length both in S/C and P/C ranges. The success of the present experiments has allowed us to design dummy blades for the cascade experiments to be conducted in the following phase of the present work for FY 1981.

ACKNOWLEDGMENT

This research was carried out under the Naval Sea Systems Command, General Hydromechanics Research Program, administered by the David Taylor Naval Ship Research and Development Center, Contract N00014-79-C-0234-P0001.

1.0 INTRODUCTION

Recently a theory for predicting the off-design performance of cavitating propellers was developed by Furuya (1976, 1978) and Furuya and Maekawa (1979) based on the supercavitating and partially cavitating cascade theories. The results of the theory compared favorably with experimental data except for the large J-range at which the partially cavitating condition prevails over the propeller blades. A question did arise as to the accuracy of the supercavitating and partially cavitating cascade theories of Furuya (1975) and Furuya and Maekawa (1979) which were used to form the sectional loading data in the above propeller theory. Only one experimental work for the cavitating cascade exists to date. The work was conducted by Wade and Acosta (1969) who used a plano-convex cascade blade, which is quite different from practical blade profiles used for high speed propellers.

The objective of the present study is, therefore, to conduct water tunnel experiments for cavitating cascades having practical blade profile shapes and to compare the results with the existing theories. The program was divided into two phases, Phase A and Phase B. We just completed Phase A for FY 1980, the results of which are reported herein. This phase is what is called a preparatory phase to the cascade experiment of Phase B for FY 1981. Before constructing an experimental set-up for cascade, it was imperative for us to conduct a single foil experiment to ensure the appropriateness of the blade profile and dimensions. We chose a cross-sectional profile shape of Hydronautics 7607.02 supercavitating propeller at 50% radial station. This cross section profile is made of a modified Tulin two-term camber with a blunt trailing edge (see the report of Furuya (1978) for the modifications in detail).

We fabricated a foil based on the above off-set data and conducted single-foil experiments at the High Speed Water Tunnel at the California Institute of Technology. The data were taken over a wide range of cavitation numbers covering from the fully-wetted, partially cavitating and supercavitating regimes. Although the purpose of the program was to compare theories with experiments for cascade flows, it was considered that a similar comparison for the single foil data just obtained would be interesting. Despite many years of studies for cavity flows to date, it was a surprise to learn that there existed no appropriate nonlinear theory for determining the characteristics of cavitating foils having practical foil profile shapes in the unbounded flow media. Wu and Wang (1964) applied an open-wake model for supercavitating foils, but the results for the drag force prediction were not quite satisfactory due to the choice of the flow model. Larock and Street (1965, 1968) used a more reliable wake model, i.e., Tulin's single vortex wake model to the S/C foil, but their solution method was applied either to flat-plate foils or an inverse type of camber specification. For the partially cavitating regime, not even a single nonlinear theory existed.

It was for this reason that we decided to devote our effort to the development of nonlinear partially cavitating and supercavitating theories which could be applied to any practical foil profile cases. With these theories developed, it was believed that we could fill the gap existing in the cavity flow theory regime. For the supercavitating flow, the theory of Larock and Street (1965) who applied the single vortex model was extended for general blade profile cases. On the other hand, we developed two partially cavitating flow theories, one using the double wake model and the other using the open wake model.

It must be pointed out here that the results of the present work will form the basic foundation for conducting the cascade work in Phase B. Since it was found in the present

experiment that the blade profile shape and its dimensions were appropriate, dummy blades to form a cascade configuration were already designed. Four dummy blades will be fabricated in the following phase. Furthermore, the foil used for the present experiment will be used as one of the cascade blades, i.e., the center foil for the force measurements.

In what follows, we will describe the experimental work, theory development, and data comparison between the theories and experiment.

2.0 EXPERIMENT

2.1 MODEL

The final goal of the program is to obtain the experimental data for cavitating cascades having practical blade profiles and to make comparisons with the existing nonlinear theories. As has been mentioned in the preceding section, due to the limited time and funding we decided to devote the first phase of the program mainly to a single-foil study which will form a basis for the study of the cascade configuration to be conducted in the following phase.

The difference between the present work and numerous previous works lies in the fact that the present one investigated the hydrodynamic characteristics for foils having practical blade profile shapes. By "practical" we mean that the blade profile must be different from flat-plate or circular arc profile shapes. For achieving the purpose, the cross-section profile of Hydronautics 7607.02 S/C propeller at 50% radial station (r = .5) was chosen. The upper and lower blade off-set data are given in Table 2.1 (see also Bohn and Altman (1976)). The reasons for choosing the cross-section profile at r = .5 were based on the solidity and stagger angle of the propeller which would be readily implemented in the High Speed Water Tunnel (HSWT) at the California Institute of Technology. In order to carry out the cascade experiment, at least five blades will be desired. By choosing the chord length of the blade to be 3.2 inches, the high solidity (sol) such as sol = 1 will possibly be achieved. Since the two-dimensional test section available at HSWT was made to have the stagger angle of 45°, that of the Hydronautics 7607.02 S/C propeller at r = .5 which is 48.9° (see Furuya (1978) for more details) matches well with this number. As far as the practicality of the blade profile is concerned, the profile chosen here is essentially a Tulin's two-term camber but with the leading edge ($x \leq 0.2$)

and trailing edge ($x \geq 0.8$) slightly modified. The report by Furuya (1978) describes these modifications in detail.

The blade set-up to the tunnel wall is shown in Figure 2.1. Two pressure taps were placed on the model. One was placed at 20% chord from the leading edge on the suction side to measure the pressure inside the cavity and the other at the base of the foil to measure the base pressure inside the wake.

Grooves were milled in the upper surface, and 1/16 inch outer diameter brass tubes were laid in these grooves. Transparent epoxy resin was molded into the grooves, completely covering the brass tubes, and then ground-smoothed with the curved plane of the upper surface of the model. Holes of 0.020 inch diameter were drilled at the specified pressure tap locations.

The high lifting force expected at the partially cavitating and the fully wetted condition required the use of the heat treated stainless steel 17-4PH. The model was fabricated and measured to an accuracy of $\pm$ 0.002 inches. The leading edge is specified to be sharp, however, sharpness in the most physically possible sense.

The cascade experiment to be conducted in the following phase simply requires dummy blades which will be mounted to the other side of the tunnel test section. These dummy blades have already been designed (see Figure 2.2) and are ready for fabrication. Four dummy blades with the center blade (just used for the present experiment) will form the cascade configuration with a solidity of unity. However, with only three blades used, i.e., two dummy blades plus the center blade, we can construct a cascade having a solidity of 0.5.

2.2 EXPERIMENTAL SET-UP AND APPARATUS

The experiments were conducted in the High Speed Water Tunnel (HSWT) of the Hydrodynamics Laboratory at the California Institute of Technology. The tunnel is a closed circuit water tunnel having an available pump power of approximately 350 hp to drive water through the working section at various controlled pressures. The speed of the water flow in the working section of the tunnel can be varied from a very low value of a foot per second up to the maximum of 80 ft/sec. More basic features of the water tunnel are discussed at length in Knapp et. al. (1948) and Ward (1976).

For this experiment, we used the two-dimensional working section, the dimensions of which are 30 inches high, 50 inches long, and 6 inches wide. In our experiment, the two-dimensional working section was installed by rotating 90°, thus horizontally, to avoid a large static pressure gradient, a particular concern for the upcoming cascade experiment.

The foil was mounted to a base fixture, fitted with a balance port fairing disk. The force balance available for the HSWT has a low and a high force range capacity. The experiment used the low range load cells having a range of $\pm$ 200 lbs. lift, $\pm$ 80 lbs. of drag and $\pm$ 300 in-lb. of moment. The accuracy of each cell is within $\pm$ 0.25% of the rated load. This accuracy is inclusive of all hysteresis, non-linearity, and repeatability.

The force balance data as well as the water tunnel flow velocity and pressure were stored in the buffer of the electronic data acquiring system at the HSWT and punched on regular IBM cards. These cards were conveniently used as input data for data reduction. The data acquisition system also has an integration capability for the force data over any time duration so that the time averaged static forces can be

recorded. The force balance accuracy mentioned before included the stability of all the electronics used in this system.

The tip clearance, which is the space between the tip of the foil and the opposite wall, was adjusted to approximately 0.07 inches to avoid wall contact when the tunnel pressure is reduced to the minimum value.

2.3 PROCEDURE

The model was set at angles of attack α = 0, 2, 4, 6, 8, and 10° at zero water velocity. Then the water velocity was increased to q_1 = 20 ft/sec or 30 ft/sec, depending upon the angle of incidence. Originally all the runs were scheduled with 30 ft/sec, however, the large force increase at the transition region between the partial cavitating and supercavitating conditions forced us to reduce the water velocity down to 20 ft/sec, particularly at the higher incidence angles, α = 8° and 10°.

The pressure in the working section was then gradually decreased from the atmospheric pressure until the cavity started appearing at the leading edge of the blade and finally choked the tunnel. The lift and drag data were taken along with the top and side photographs. All the force measurements were time averaged over 2 seconds. The top photographs were taken with 4 x 5 inch professional film centered at approximately 3.7 chord length downstream of the model. The side photographs were taken with 35-mm film centered approximately 3.6 chord length downstream of the model. Both photographs were synchronized by the strobe light. The lengths of cavities were measured from these photographs.

The water speed was determined from the pressure difference between the test section and the constant cross-sectional area at the upstream of the contracting nozzle. The pressure

difference was measured by a mercury manometer. The static pressure of the tunnel test section was also measured at the top of the section by means of a mercury manometer.

The vapor pressure of water was used for the calculation of the approximate cavitation number, but was corrected for presentation of the experimental data. More details will be discussed in the following section.

2.4 DATA REDUCTION

Various corrections were made on the cavitation numbers and the results of the force measurements. The cavitation number based on the cavity pressure is defined

$$\sigma = \frac{p_1 - p_c}{\frac{1}{2}\rho q_1^2}$$

where p_1 is the static pressure at the center of the test section (3 inches from the top and 3 inches from the bottom), ρ is the density of water, q_1 is the velocity of the water at the test section, and p_c is the cavity pressure. On the other hand, the cavitation number based on the water vapor pressure is defined

$$\sigma_v = \frac{p_1 - p_v}{\frac{1}{2}\rho q_1^2}$$

where p_v is the vapor pressure of water at the temperature during the experiment. Initially, we had planned to measure the pressure inside the cavity by using one of the pressure taps mounted on the foil. However, we had difficulty in doing so, particularly for short cavity cases. Also, when the tunnel pressure was reduced to small values, there existed an air leakage problem, which caused an error in measurement. We had a very short tunnel time assigned and there was no time for repair.

It was, therefore, decided to make corrections on σ_v's to provide all the data in terms of σ's. The correlation between σ and σ_v was presented by Kermeen (1956) and Wade and Acosta (1965) and this was used for the present purpose. Some of the measured cavity pressure data were utilized for justifying this correction method. Due to the lack of correction data in the region $\sigma > 1.5$, the cavitation numbers are left uncorrected. It must be mentioned that the use of uncorrected cavitation numbers for large σ's will not greatly affect the force data presentation since the force is fairly flat as a function of σ.

The measured forces were normalized

$$C_L = \frac{\text{Lift}}{\frac{1}{2}\rho q_1^2 A}$$

$$C_D = \frac{\text{Drag}}{\frac{1}{2}\rho q_1^2 A}$$

where A is the plan form area of the model. First it was found that the influence of the pressure change of the tunnel during the experiment on the force balance reading was confirmed to be negligibly small. Also, based on the previous literature such as that of Barker and Ward (1976), very slight corrections were made for the measured lifting forces. Thus, only the drag forces were corrected. The corrections included the viscous drag on the model and the fairing disk. Over the tested water velocity range, the boundary layer is considered to be predominantly laminar. The viscous drag on the model and fairing disk was estimated by the Blasius boundary layer equation. The wetted areas for this correction are varied depending on the fully wetted, partially cavitating, or supercavitating.

The wall effects for the cavity flows in solid wall tunnels are discussed by Whitney and Brennen (1969) and Baker (1972). Since the method of Baker (1972) indicated such a correction

to be small for our tunnel set-up, the data were left uncorrected for the wall effect.

All other corrections, such as buoyancy, wall boundary layer interference, solid blockage and wake blockage were not included.

3.0 THEORY DEVELOPMENT

3.1 SUPERCAVITATING FLOW THEORY

Figure 3.1 shows a flow configuration of a two-dimensional supercavitating foil. In order to represent the cavity termination and highly turbulent flow subsequent to it, the single spiral vortex model of Tulin (1964) is employed. On the blade the cavity is assumed to spring from the sharp leading edge B and trailing edge T, both fixed but arbitrary, extended downstream. The pressure inside the cavity is taken to be constant, p_c. The blade reference coordinate is inclined at an angle of α in an undisturbed flow so that the incoming uniform flow is always fixed to be parallel to the x-axis of the coordinate system. There exists a reason for not inclining the flow angle but instead tilting the foil. The reason will be described during the course of the theory development. The origin of the coordinate is placed at the leading edge of the blade with x-axis parallel to the undisturbed flow. The wetted portion of the blade is defined by $y = f(x)$ or by its inclination $\beta = \tan^{-1}\left(\frac{df(x)}{dx}\right)$. The physical flow field is mapped onto the potential plane W as shown in Figure 3.2. The complex potential of the stagnation point is chosen to be (0,0) in this transformation. The potential plane is then transformed onto the upper half of a new plane $\zeta = \xi + i\eta$ of Figure 3.3 by a mapping function

$$\zeta = a\sqrt{\frac{W}{\Phi_L - W}} \tag{3.1}$$

or

$$W = \frac{\Phi_L \zeta^2}{a^2 + \zeta^2}. \tag{3.2}$$

The cavity end point is mapped to infinity and the infinity point in z or W plane is now mapped onto a point $\zeta = ia$.

A hodograph variable ω is introduced

$$\frac{dW}{dz} = q\, e^{-i\theta} = q_c\, e^{-i\omega}$$

where q and θ are the magnitude and direction of the flow velocity. Thus

$$\omega = \theta + i\tau$$

where

$$\tau = \ln\left(\frac{q}{q_c}\right)$$

and

$$q_c = \sqrt{1 + \sigma}\; q_1 \;,\quad \sigma = \frac{p_1 - p_c}{\frac{1}{2}\rho q_1^{\,2}}$$

where the uniform flow velocity q_1 is taken to be unity throughout the present analysis.

The boundary conditions on the real-axis ξ are now expressed either in terms of θ or τ;

(i) $\tau = 0$, $-\infty < \xi < -1$ and $b < \xi < \infty$,
(ii) $\theta = \beta$, $-1 < \xi < 0$,
(iii) $\theta = \pi + \beta$, $0 < \xi < b$.

This is a typical mixed-type boundary value problem, and the solution for ω is readily written

$$\omega(\zeta) = \sqrt{(\zeta + 1)(\zeta - b)} \left\{ \frac{1}{2\pi i} \int_{-1}^{b} \frac{2\beta}{i\sqrt{(1 + \xi')(b - \xi')}} \frac{d\xi'}{\xi' - \zeta} \right.$$

$$\left. + \frac{1}{2\pi i} \int_{0}^{b} \frac{2\pi}{i\sqrt{(1 + \xi')(b - \xi')}} \frac{d\xi'}{\xi' - \zeta} + P \right\}, \qquad (3.3)$$

where the Cauchy principle values are taken for the integrals any time it is necessary and P is a real constant, yet to be known.

We have a total of four unknown quantities, a, b, P, Φ_L, requiring four equations to determine them uniquely.

The various boundary conditions will be applied;

(i) at infinity

$$\omega(ia) = i\ln\left(\frac{1}{\sqrt{1+\sigma}}\right): \qquad 2 \text{ equations}$$

(ii) length of arc = S: 1 equation

(iii) body-cavity system closure condition (see Larock and Street (1965)),

$$\mathrm{Re}\left\{\oint_C \omega\, dW\right\} = 0 \ : \ 1 \text{ equation.}$$

Application of these conditions to Equation (3.3) yields the following four equations:

(i) at upstream infinity:

$$\begin{Bmatrix} f_1 \\ f_2 \end{Bmatrix} \equiv \sqrt{(ia+1)(ia-b)} \left\{ \frac{1}{2\pi i} \int_{-1}^{b} \frac{2\beta}{i\sqrt{(1+\xi')(b-\xi')}} \frac{d\xi'}{\xi'-ia} \right.$$

$$\left. + \frac{1}{2\pi i} \int_{0}^{b} \frac{2\pi}{i\sqrt{(1+\xi')(b-\xi')}} \frac{d\xi'}{\xi'-ia} + P \right\} - i\ln\left(\frac{1}{\sqrt{1+\sigma}}\right) = 0$$

or

$$f_1 \equiv \mathrm{Re}\left\{\omega(ia)\right\} = 0 \tag{3.4}$$

$$f_2 \equiv \mathrm{Im}\left\{\omega(ia)\right\} - \ln\left(\frac{1}{\sqrt{1+\sigma}}\right) = 0. \tag{3.5}$$

(ii) wetted arc length = S:
On the wetted part of the streamline,

$$\frac{dz}{ds} = e^{i\beta},$$

or

$$ds = e^{-i\beta}\,\frac{e^{i\omega}}{q_c}\,\frac{dW}{d\xi}\,d\xi. \tag{3.6}$$

For $-1 < \xi < b$, $\omega(\xi)$ can be written as follows:

$$\omega(\xi) = \begin{cases} i\,g(\xi) + \beta(\xi), & -1 < \xi < 0 \\ i\,g(\xi) + \beta(\xi) + \pi, & 0 < \xi < b \end{cases}$$

where

$$g(\xi) = \sqrt{(1+\xi)(b-\xi)}\left\{-\frac{1}{\pi}\oint_{-1}^{b}\frac{\beta(\xi')}{\sqrt{(1+\xi')(b-\xi')}}\,\frac{d\xi'}{\xi'-\xi}\right.$$

$$\left. -\int_{0}^{b}\frac{1}{\sqrt{(1+\xi')(b-\xi')}}\,\frac{d\xi'}{\xi'-\xi} + P\right\}, \tag{3.7}$$

and $\oint$ indicates a Cauchy principle integral. By integrating Equation (3.6) we obtain

$$s(\xi) = \int_{\xi}^{b} sg(\xi)\,\frac{e^{-g(\xi)}}{\sqrt{1+\sigma}}\,\frac{dW}{d\xi}\,d\xi \tag{3.8}$$

where

$$sg(\xi) = \begin{cases} 1 & , \ \xi > 0 \\ -1 & \xi < 0 \end{cases} .$$

The arc length condition is therefore satisfied by the following equation:

$$f_3 \equiv S - s(-1) = 0 \tag{3.9}$$

(iii) closure condition:
For zero net source strength within the contour C enclosing the body-cavity system this can be written

$$Re\left\{ \oint_C \omega(\zeta)\, dW \right\} = 0. \tag{3.10}$$

And, after transformation (see p. 173 of Larock and Street (1965)),

$$Re\left\{ \oint_C \omega(\zeta)\, \frac{dW}{d\zeta}\, d\zeta \right\} = 0 \tag{3.11}$$

where

$$\frac{dW}{d\zeta} = \frac{2a^2 \Phi_L \zeta}{(\zeta^2 + a^2)^2} .$$

Since C has a double pole at $\zeta = ia$, the closure condition becomes

$$Re\left\{ \frac{d\omega(\zeta)}{d\zeta} \Big|_{\zeta = ia} \right\} = 0$$

or

$$f_4 \equiv Re\left\{\omega'(ia)\right\} = Re\left\{ \frac{H'(ia)}{H(ia)}\, \omega(ia) + H(ia)\, G'(ia) \right\} = 0 \tag{3.12}$$

where

$$H = \sqrt{(\zeta + 1)(\zeta - b)}$$

and G is the remaining part of the right hand side of Equation (3.3).

A set of four nonlinear equations just obtained, i.e., (3.4), (3.5), (3.9) and (3.12), will determine the four unknown solution parameters.

It must be mentioned here that when one applies the transformation formula for the closure condition from Equation (3.10) to Equation (3.11), it will become

$$\mathrm{Re}\left[e^{-i\alpha_1}\left\{\frac{d\omega(\zeta)}{d\zeta}\bigg|_{\zeta = ia}\right\}\right] = 0.$$

Therefore, if there exists a finite incoming flow angle, the closure condition takes a different form from Equation (3.10). This is the reason for maintaining the zero-incoming flow set-up as has been mentioned earlier.

The lift and drag coefficients, C_L and C_D, on a super-cavitating hydrofoil will be obtained in the following manner. Defining C_L and C_D as follows,

$$C_L = \int_0^{\text{chord}} \frac{(p - p_c)}{\frac{1}{2}\rho q_1^2}\, dx$$

$$C_D = \int_0^{\text{chord}} \frac{(p - p_c)}{\frac{1}{2}\rho q_1^2}\, dy$$

Or we can write

$$C_L = q_c^2 \int_{-1}^{b} \left(1 - \frac{q^2}{q_c^2}\right) \cdot \frac{dx}{ds} \cdot \frac{ds}{d\xi}\, d\xi$$

where

$$q_c^2 = 1 + \sigma$$

$$C_{p_c} \equiv \frac{p - p_c}{\frac{1}{2}\rho q_c^2} \equiv 1 - \frac{q^2}{q_c^2} = 1 - \left[\exp\left\{\mathrm{Im}(\omega(\xi))\right\}\right]^2$$

$$\mathrm{Im}\left\{\omega(\xi)\right\} = g(\xi) \text{ in Equation (3.7)},$$

$$\frac{dx}{ds} = \cos\beta ,$$

$$\frac{ds}{d\xi} = -sg(\xi)\ \frac{e^{-g(\xi)}}{\sqrt{1+\sigma}} .$$

Similarly,

$$C_D = \int_{-1}^{b} C_p \frac{dy}{ds} \cdot \frac{ds}{d\xi'}\, d\xi'$$

where

$$\frac{dy}{ds} = \sin\beta .$$

3.2 PARTIALLY CAVITATING FLOW THEORY

3.2.1 Double Wake Model

One of the most difficult problems in formulating a cavitating flow theory lies in construction of the flow configuration. The degree of difficulty increases in the partially cavitating flow, particularly for the flow around the foil having a blunt trailing edge. The turbulent wake behind the foil must be treated in a somewhat different manner from the cavity itself. In the present theory we applied a "double wake" model as is shown in Figure 3.4. In this model the wake consists of two parts, i.e., the near wake and the far wake. Inside the far wake the dynamic pressure is gradually recovered towards the

infinity whereas that of the near wake is somewhat in between p_1 and p_c. In terms of the velocity, the near wake wall velocity is thus expressed as follows

$$q_w = q_c \left(\frac{\ell_c}{c}\right) + q_1 \left\{1 - \left(\frac{\ell_c}{c}\right)\right\}. \tag{3.13}$$

As was described in the report of Furuya and Maekawa (1979), we have another reason for using the formula (3.13). When one calculates the force coefficients of cavitating hydrofoils having blunt trailing edges, it is preferable to have a smooth transition between the partially cavitating and supercavitating conditions. Equation (3.13) allows us to smoothly blend the partially cavitating flow into the S/C flow. The near wake wall velocity is gradually equated to q_c as ℓ_c approaches the chord length.

The physical flow field shown in Figure 3.4 is mapped onto the potential plane shown in Figure 3.5 As is shown in this potential plane of Figure 3.5, the velocity q and flow angle θ on the upper and lower far wake boundaries are assumed to have the identical values for the same potential ϕ. This also requires the condition that ϕ at the upper cavity end point is equal to ϕ at the lower cavity end point. It is realized that this is identical to the single spiral vortex model of Tulin (1964) used for the present double wake flow configuration. The potential plane is once more transferred onto the upper half of the ζ-plane with a mapping function

$$\zeta = a \sqrt{\frac{W}{\Phi_w - W}}$$

or

$$W = \frac{\Phi_w \zeta^2}{a^2 + \zeta^2}. \tag{3.14}$$

where Φ_w denotes the potential at the point corresponding to the cavity end point and $\zeta = ia$ corresponds to the infinity in the physical plane.

The boundary conditions on the real-axis ξ are now expressed

$$\text{(i)} \quad \tau = 0 \qquad , \quad -\infty < \xi < -1 \, , \; f < \xi < \infty \, ,$$

$$\text{(ii)} \quad \tau = \ln \frac{\sqrt{1+\sigma}}{q_w} \qquad , \quad b < \xi < c \, ,$$

$$\text{(iii)} \quad \theta = \begin{cases} \beta_1 \left(\equiv \tan^{-1} \dfrac{dy}{dx} \right) & , \quad -1 < \xi < 0 \\ \beta_1 + \pi & , \quad 0 < \xi < b \\ \beta_2 + \pi & , \quad c < \xi < f. \end{cases}$$

The solution for ω will be obtained

$$\omega(\zeta) = \sqrt{\frac{(\zeta+1)(\zeta-b)(\zeta-f)}{\zeta-c}} \left\{ \frac{1}{2\pi i} \left[\int_{-1}^{b} \frac{2\beta_1}{i\sqrt{\dfrac{(\xi'+1)(b-\xi')(\xi'-f)}{\xi'-c}}} \frac{d\xi'}{\xi'-\zeta} \right. \right.$$

$$+ \int_{0}^{b} \frac{2\pi}{i\sqrt{\dfrac{(\xi'+1)(b-\xi')(\xi'-f)}{\xi'-c}}} \frac{d\xi'}{\xi'-\zeta}$$

$$+ \int_{b}^{c} \frac{2i \ln \left(\dfrac{\sqrt{1+\sigma}}{q_w} \right)}{\sqrt{\dfrac{(\xi'+1)(\xi'-b)(\xi'-f)}{\xi'-c}}} \frac{d\xi'}{\xi'-\zeta}$$

$$\left. \left. + \int_{c}^{f} \frac{2(\beta_2+\pi)}{i\sqrt{\dfrac{(\xi'+1)(\xi'-b)(f-\xi')}{\xi'-c}}} \frac{d\xi'}{\xi'-\zeta} \right] + P \right\} . \qquad (3.15)$$

By taking σ as one of the unknown parameters, we have a total of seven unknown quantities, i.e., a, b, c, f, σ, P, ϕ_w, requiring seven equations to determine them uniquely.

Boundary conditions which have not been used yet will be applied as follows:

(i) at infinity ($\zeta = ia$)

$$\omega(ia) = i \ln\left(\frac{1}{q_w}\right) \quad : \text{ 2 equations}$$

(ii) length of the first arc = S_1

$$S_1 = s_1(-1) \text{ where } s_1 \text{ in Eqn. (3.18)} \quad : \text{ 1 equation}$$

(iii) length of the second arc = S_2

$$S_2 = s_2(-1) \text{ where } s_2 \text{ in Eqn. (3.22)} \quad : \text{ 1 equation}$$

(iv) cavity end lands on the upper surface of the blade : 1 equation

(v) cavity length matches the specified length: 1 equation

(vi) foil-cavity-wake system closure condition

$$\mathrm{Re}\left\{\oint_C \omega dW\right\} = 0. \quad : \text{ 1 equation}$$

Application of these conditions to Equation (3.15) yields the following seven equations:

(i) at the infinity ($\zeta = ia$);

$$\begin{Bmatrix} f_1 \\ f_2 \end{Bmatrix} \equiv \sqrt{\frac{(ia+1)(ia-b)(ia-f)}{ia-c}}$$

$$\times \left\{ -\frac{1}{\pi} \int_{-1}^{b} \frac{\beta_1}{\sqrt{\frac{(\xi'+1)(b-\xi')(\xi'-f)}{\xi'-c}}} \frac{d\xi'}{\xi'-ia} \right.$$

$$-\int_0^b \frac{1}{\sqrt{\frac{(\xi'+1)(b-\xi')(\xi'-f)}{\xi'-c}}} \frac{d\xi'}{\xi'-ia}$$

$$+\frac{1}{\pi}\ln\left(\frac{\sqrt{1+\sigma}}{q_w}\right)\int_b^c \frac{1}{\sqrt{\frac{(\xi'+1)(\xi'-b)(\xi'-f)}{\xi'-c}}} \frac{d\xi'}{\xi'-ia}$$

$$-\frac{1}{\pi}\int_0^f \frac{\beta_2+\pi}{\sqrt{\frac{(\xi'+1)(\xi'-b)(f-\xi')}{\xi'-c}}} \frac{d\xi'}{\xi'-ia} + P\Bigg\} - i\ln\left(\frac{1}{q_w}\right) = 0,$$

or

$$f_1 \equiv \mathrm{Re}\{\omega(ia)\} = 0 \qquad (3.16)$$

$$f_2 \equiv \mathrm{Im}\{\omega(ia)\} - \ln\left(\frac{1}{q_w}\right) = 0. \qquad (3.17)$$

(ii) first arc = S_1;

On the wetted part of the streamline,

$$\frac{dz}{ds_1} = e^{i\beta_1}$$

$$ds_1 = e^{-i\beta_1}\frac{e^{i\omega}}{q_w}\frac{dW}{d\xi}\,d\xi$$

For $-1<\xi<b$, $\omega(\zeta)$ can be written as follows:

$$\omega(\xi) = \begin{cases} ig_1(\xi)+\beta_1(\xi), & -1<\xi<0 \\ ig_1(\xi)+\beta_1(\xi)+\pi, & 0<\xi<b \end{cases}$$

where

$$g_1(\xi) = \sqrt{\frac{(\xi+1)(b-\xi)(\xi-f)}{\xi-c}}\ X$$

$$\times \left\{ -\frac{1}{\pi} \int_{-1}^{b} \frac{\beta_1}{\sqrt{\frac{(\xi'+1)(b-\xi')(\xi'-f)}{\xi'-c}}} \frac{d\xi'}{\xi'-\xi} \right.$$

$$- \int_{0}^{b} \frac{1}{\sqrt{\frac{(\xi'+1)(b-\xi')(\xi'-f)}{\xi'-c}}} \frac{d\xi'}{\xi'-\xi}$$

$$+ \frac{1}{\pi} \ln\left(\frac{\sqrt{1+\sigma}}{q_w}\right) \int_{b}^{c} \frac{1}{\sqrt{\frac{(\xi'+1)(\xi'-b)(\xi'-f)}{\xi'-c}}} \frac{d\xi'}{\xi'-\xi}$$

$$\left. - \frac{1}{\pi} \int_{c}^{f} \frac{\beta_2 + \pi}{\sqrt{\frac{(\xi'+1)(\xi'-b)(f-\xi')}{\xi'-c}}} \frac{d\xi'}{\xi'-\xi} + P \right\}.$$

Therefore,

$$s_1(\xi) = \int_{\xi}^{b} sg(\xi) \frac{e^{-g_1(\xi)}}{q_w} \frac{dW}{d\xi} d\xi \qquad (3.18)$$

where

$$sg(\xi) = \begin{cases} 1, & \xi > 0 \\ -1, & \xi < 0 \end{cases}$$

and

$$\frac{dW}{d\xi} = a^2 \phi_w \frac{2\xi}{(a^2+\xi^2)^2}. \qquad (3.19)$$

Thus

$$f_3 \equiv S_1 - s_1(-1) = 0 \qquad (3.20)$$

(iii) length of the second arc = S_2 ;

$$f_4 \equiv S_2 - s_2(f) = 0 \tag{3.21}$$

where

$$s_2(\xi) = \int_c^{\xi} \frac{e^{-g_2(\xi)}}{q_w} \frac{dW}{d\xi'}\, d\xi' \tag{3.22}$$

and

$$g_2(\xi) = \sqrt{\frac{(\xi+1)(\xi-b)(f-\xi)}{\xi-c}}$$

$$\times \left\{ -\frac{1}{\pi} \int_{-1}^{b} \frac{\beta_1}{\sqrt{\frac{(\xi'+1)(b-\xi')(\xi'-f)}{\xi'-c}}} \frac{d\xi'}{\xi'-\xi} \right.$$

$$- \int_0^b \frac{1}{\sqrt{\frac{(\xi'+1)(b-\xi')(\xi'-f)}{\xi'-c}}} \frac{d\xi'}{\xi'-\xi}$$

$$+ \frac{1}{\pi} \ln\left(\frac{\sqrt{1+\sigma}}{q_w}\right) \int_b^c \frac{1}{\sqrt{\frac{(\xi'+1)(b-\xi')(\xi'-f)}{\xi'-c}}} \frac{d\xi'}{\xi'-\xi}$$

$$\left. - \frac{1}{\pi} \int_c^f \frac{\beta_2 + \pi}{\sqrt{\frac{(\xi'+1)(\xi'-b)(f-\xi')}{\xi'-c}}} \frac{d\xi'}{\xi'-\xi} + P \right\}.$$

(iv) cavity closure condition;

$$f_5 \equiv y_C - f_u(x_C) = 0, \tag{3.23}$$

where f_u is upper surface shape of the foil

where

$$x_C = x_B + \frac{1}{\sqrt{1+\sigma}} \int_b^c \cos g_c(\xi') \frac{dW}{d\xi'} d\xi'$$

$$y_C = y_B + \frac{1}{\sqrt{1+\sigma}} \int_b^c \sin g_c(\xi') \frac{dW}{d\xi'} d\xi' ,$$

$$g_c(\xi) = \sqrt{\frac{(\xi+1)(\xi-b)(f-\xi)}{c-\xi}}$$

$$\times \left\{ -\frac{1}{\pi} \int_{-1}^{b} \frac{\beta_1(\xi')}{\sqrt{\frac{(\xi'+1)(b-\xi')(\xi'-f)}{\xi'-c}}} \frac{d\xi'}{\xi'-\xi} \right.$$

$$- \int_0^b \frac{1}{\sqrt{\frac{(\xi'+1)(b-\xi')(\xi'-f)}{\xi'-c}}} \frac{d\xi'}{\xi'-\xi}$$

$$+ \frac{1}{\pi} \ln\left(\frac{\sqrt{1+\sigma}}{q_w}\right) \int_b^c \frac{1}{\sqrt{\frac{(\xi'+1)(\xi'-b)(\xi'-f)}{\xi'-c}}} \frac{d\xi'}{\xi'-\xi}$$

$$\left. - \frac{1}{\pi} \int_c^f \frac{\beta_2 + \pi}{\sqrt{\frac{(\xi'+1)(\xi'-b)(f-\xi)}{\xi'-c}}} \frac{d\xi'}{\xi'-\xi} + P \right\}.$$

(v) length of the cavity matches the specified length

$$f_6 \equiv x_C - \ell_c = 0 \qquad (3.24)$$

Where

$$x_C = x_B + \frac{1}{\sqrt{1+\sigma}} \int_b^c \cos g_c(\xi') \frac{dW}{d\xi'} d\xi'$$

(vi) foil-cavity-wake system closure condition;
For zero source strength within the contour enclosing the system, we must have

$$\mathrm{Re}\left\{ \oint_C \omega(\zeta)\, dW \right\} = 0$$

Similar to the S/C theory, the condition reduces to

$$\mathrm{Re}\left\{ \frac{dW(\zeta)}{d\zeta}\bigg|_{\zeta = ia} \right\} = 0$$

or

$$f_7 = \mathrm{Re}\left\{ \omega'(ia) \right\} = \mathrm{Re}\left\{ \frac{H'(ia)}{H(ia)}\, \omega(ia) + H(ia)\, G'(ia) \right\} = 0. \quad (3.25)$$

where

$$H(\zeta) = \sqrt{\frac{(\zeta + 1)(\zeta - b)(\zeta - f)}{\zeta - c}}$$

and

$G(\zeta)$ = The remaining part of the right-hand side of Equation (3.15).

The lift and drag coefficients for the present case will be obtained in a slightly different way from that for the S/C foil theory. The lift L is defined as follows,

$$L = \int_0^{\text{chord}} (p_\ell - p_u)\, dx$$

where p_ℓ and p_u denote the pressures on the lower and upper portion of the foil, respectively. Then, the normalization will provide the lift coefficient C_L

$$C_L = \frac{L}{\frac{1}{2}\rho q_1^2 \cdot \text{chord}} = \int_0^1 \frac{p_\ell - p_1}{\frac{1}{2}\rho q_1^2 \cdot \text{chord}}\, dx \; - \int_0^1 \frac{p_u - p_1}{\frac{1}{2}\rho q_1^2 \cdot \text{chord}}\, dx .$$

Evaluation will be made in the transform plane, i.e.,

$$C_L = -\int_{-1}^{b} C_p \frac{dx}{ds_1} \frac{ds_1}{d\xi} d\xi \; - \int_{c}^{f} C_p \frac{dx}{ds_2} \frac{ds_2}{d\xi}\, d\xi + \sigma \cdot \left({}^{\ell c}/_{c}\right) \qquad (3.26)$$

where

$$C_p = 1 - {}^{q^2}/_{q_1 2}$$

$$\frac{q^2}{q_1^2} = \frac{q_w^2}{q_1^2} \cdot \frac{q^2}{q_w^2} = q_w^2 \cdot e^{2\,\mathrm{Im}\{\omega(\xi)\}}$$

$$\frac{dx}{ds_1} = \cos \beta_1$$

$$\frac{dx}{ds_2} = \cos \beta_2$$

$$\frac{ds_1}{d\xi} = -sg(\xi)\, \frac{e^{-g_1(\xi)}}{q_w} \frac{dW}{d\xi}$$

$$\frac{ds_2}{d\xi} = \frac{e^{-g_2(\xi)}}{q_w} \frac{dW}{d\xi}$$

$$\frac{dW}{d\xi} = \text{Eqn. (3.19)}.$$

Similarly, the drag coefficient C_D will be given

$$C_D = \int \frac{p - p_w}{\frac{1}{2}\rho q_1^2 \cdot \text{chord}}\, dy$$

$$= \frac{1}{\text{chord}} \left[\int_{-1}^{b} C_p \frac{dy}{ds_1} \frac{ds_1}{d\xi} \, d\xi + \int_{C}^{f} C_p \frac{dy}{ds_2} \frac{ds_2}{d\xi} \, d\xi + I_1 + I_2 \right] \quad (3.27)$$

$$I_1 = \int_{\text{cavity}} \frac{p_2 - p_1}{\frac{1}{2}\rho q_1^2} \, dy = -\sigma \cdot y_c$$

$$I_2 = \int_{\substack{\text{base} \\ \text{thickness}}} \frac{p_1 - p_w}{\frac{1}{2}\rho q_1^2} \, dy = -C_{pw} \cdot (\text{foil base thickness}),$$

where

$$\frac{dy}{ds_1} = \sin \beta_1$$

$$\frac{dy}{ds_2} = \sin \beta_2$$

y_c = the y-coordinate of the cavity end point

$$C_{pw} = \frac{p_w - p_1}{\frac{1}{2}\rho q_1^2} .$$

Like any other nonlinear theory, it is a hard task to obtain the first numerically converged solution for a posed problem. Once it is obtained, the change of incidence angle, cavity length and/or blade profile shape will not provide any difficulty in finding the solution with the already obtained solution used as a starting point for the iteration loop. The present partially cavitating theory with the double wake model was the most difficult theory for finding the first converged solution. It took us many months of computer program debuggings and trials. It was finally found that Equation (3.25) has a behavior similar to $(\log a)/a$ with respect to "a" for all other parameters fixed. It means that this function has two roots for "a", i.e., 1 and ∞. Therefore, if the initial guess for "a" is large, Newton's

method calculates the slope for convergence in totally the opposite direction and finds ∞ to be the solution. This fact was discovered by plotting various multidimensional functions for each parameter. By starting a rather small value for "a", the convergence for the iteration loop was immediately obtained. The computer cost of calculating the solution for one problem was about $15 with the 7600 CDC computer at the Lawrence Berkeley Laboratory.

3.2.2 Open Wake Model

This "open wake model" is a rather simple model, as is shown in Figure 3.7 which is similar to that used for partially cavitating plano-convex cascade flows (see Furuya (1978)). In this model it is assumed that the pressure behind the foil immediately recovers that of the uniform flow and continues to the downstream infinity. This wake is considered not to close and thus is called here "open wake model".

The technique of solving the problem with this model is identical to the previous one, first mapped onto the potential plane W in Figure 3.8 and then ζ-plane in Figure 3.9. Since this model and the previous one are almost identical in the mathematical formulation, only the differences will be described in the following. The first one is the mapping function between the W-plane and ζ-plane, i.e.,

$$W = \tilde{A}\zeta^2, \tag{3.28}$$

therefore $dW/d\xi$ in various equations of the previous section should be replaced by

$$\frac{dW}{d\xi} = 2\tilde{A}\xi. \tag{3.29}$$

The second difference is that the constant term P for ω in Equation (3.15) must be zero. This condition stems from the fact that ω should be finite as $\zeta \to \infty$ since the infinity point

in the ζ-plane corresponds to the infinity point in the physical plane z. This point is quite different from the double wake model in which the infinity point in the ζ-plane corresponds to the end point of cavity where the logarithmic singularity is allowed to exist.

The third one is associated with the normalization velocity in the definition for ω. Since the wake velocity q_w is assumed to be q_1 in the present model,

$$\frac{dW}{dz} = qe^{-i\vartheta} = q_1 e^{-i\omega} \tag{3.30}$$

where q_1 is normalized to be unity. It means that all q_w's in the previous flow model should be replaced by one.

The number of unknown parameters here is only five, i.e., $\tilde{A}$, b, c, f, σ. Boundary conditions for determining these parameters include (i) through (v) of the double wake model case, excluding the closure condition. It must be mentioned that only one condition is available from (i) since the imaginary part of ω as $\zeta \to \infty$ is always zero. Furthermore, a slight modification was made here for the condition (iv) in Equation (3.23). Instead of the end point of cavity landing right on the upper part of the blade, we introduced the turbulent boundary layer thickness after cavity collapse into this condition. Therefore, this condition now reads

$$f_5 \equiv y_c - (f_u(x_c) + y_\vartheta) = 0 \tag{3.31}$$

where

y_ϑ = turbulent boundary layer thickness.

This concept was tried for the double wake model. However, it had very little effect on the final flow characteristics determined and thus was not explained in the previous section. The selection for y_ϑ is arbitrary and will only be determined

based on experimental data. This concept has been introduced simply on the trial basis for the partially cavitating flow theory and will require a further refinement for more rigorous application. We can use the same formula for the force coefficient calculations as those described for the double wake model simply by applying the changes of Equations (3.29) and (3.30).

4.0 RESULTS

4.1 FLOW OBSERVATION

Figures 4.1 through 4.5 show various flow patterns with the cavitation number reduced at angles of incidence 0° to 10° with 2 degrees increment. The top and side views of these photos were taken simultaneously by using a strobe light method. The duration of light was about 10 microseconds. The cavitation numbers used for presenting the results are those corrected according to the method mentioned in Section 2.4 so that they must be close to the actual pressure inside the cavity. We ensured this point by comparing these corrected cavitation numbers with those of measurement for several cases. It must be mentioned that we were unable to use the measured cavity pressures throughout the present study since the data became unreliable due to the air leakage of the line. This experimental problem could not be repaired during the short period of tunnel time available to us.

At α = 0°, it is seen from Figure 4.1 that the cavity starts at the foil base and stays there all the way until the tunnel choking condition. We can observe several cavitation streaks of finger-type starting from the leading edge at smaller cavitation numbers but should categorize this flow as a base-cavitated flow. At α = 2°, the cavitation now occurred both from the leading edge and trailing edge. At an σ of about .35, these two cavities merged together and thus the flow pattern became a supercavitating condition. The flow phenomena observed at the time of merging was rather abrupt. One of the original objectives of the present study was to investigate the discrepancy between the theory and experiment for a supercavitating propeller. The discrepancy appeared in a comparison for the thrust coefficient at a higher advance speed range (see the report of Furuya (1978)). This is the range of J at which the blade will experience the partial cavitation since the local

flow incidence angles at each blade section become small, e.g., $0° \sim 2°$. In the analysis of Furuya (1978) we assumed a regular, single partial cavity, whereas the experiment showed either base-cavity or double cavity for the partial cavity occurring at $\alpha = 0° \sim 2°$. It seems quite possible that the discrepancy in the propeller performance prediction method is attributable to this erroneous perception of the flow configuration at the partially cavitating flow regime.

For the incidence angle larger than 4°, no base cavity was observed any more and all cavities started from the leading edge and grew longer with decrease in pressure. Most of the cavities observed here were of bubble type. The cavity walls became clear and glassy for the cases of high incidence angle with long cavities (see Figures 4.4 (f) and 4.5 (f)).

Although we did not observe any natural instability near ℓ_c/chord = 1 such as that reported in the paper of Wade and Acosta (1967), we had difficulty in keeping the flow steady at a desired cavity length for large incidence angles during the partially cavitating condition. The phenomena will clearly be seen in Figures 4.5(c) and (d); immediately after ℓ_c/chord = 0.5 was achieved, the cavity extended abruptly beyond the chord length with a slight decrease in pressure and could not hold at any point in between them. It is for this reason that only a few data points were obtained at the p/c condition for α = 8° and 10°, as will be seen in the force data.

4.2 FORCE COEFFICIENTS

Data corrections for the measured lift and drag coefficients were made in the way explained in Section 2.4 and they are shown in Figures 4.6 and 4.7 at α = 0° through 10°. The cavitation numbers used here are again the ones with corrections and thus are supposed to be σ_{cavity}'s.

All data points taken during the experiment are shown in these figures and not a single point is excluded. Figures 4.8 and 4.9 show composite lift and drag coefficients made by interpolating the experimental data. It is seen from these figures that all lift curves show a similar trend as a function of σ except for $\alpha = 0°$ as mentioned above. It must be noted, however, that the hump near the transition point, i.e., between the S/C and P/C regimes, is the largest at $\alpha = 2°$ and gradually becomes unnoticeable as α increases.

For the supercavitating range, particularly at small cavitation numbers, the lift forces increase with the incidence angle but this relationship overturns for short cavity cases. This is the behavior which all theories, including nonlinear theories, fail to predict since the effect of cavity collapse and subsequent turbulent mixing near the foil cannot be accurately represented mathematically.

The newly developed theories, one for the supercavitating flows and two for the partially cavitating flows, were used for comparison with the experimental data. The results are shown only for the incidence angles of 4, 6 and 8 degrees in Figures 4.6 and 4.7. The supercavitating flow theory for the lift coefficient agrees well with the experiment for small cavitation numbers at which the cavity lengths are long, but underestimates them for short cavity cases. For the drag coefficients the overall prediction capability of the theory is reasonable, however, no definite trend for the discrepancy exists. This fact seems to confirm the difficulty in accurate measurements and data reduction for the drag force in this type of experiment.

For the partially cavitating regime, the two new theories provide analytical data for the lift and drag forces. The double wake model substantially underpredicted both forces, whereas the open wake model showed an accurate trend with a choice of the wake thickness y_θ in Equation (3.31) as shown in Figure

4.10. As has been mentioned earlier, it remains to be seen whether or not this choice of y_ϑ in Figure 4.10 can be applied to the other types of foils for accurate prediction of lift forces. It must be mentioned, however, that the theory showed a numerical instability as ℓ_c/c becomes greater than 0.8, similar to that reported in Furuya (1980).

It was a disappointment that the double wake model failed to predict the forces accurately. As will be seen later, the only problem of this method stems from the poor capability for predicting the cavitation number against the specified cavity length. If this were done properly, the force coefficients would be predicted accurately. It can readily be seen from the fact that the force coefficient for the partial cavity flow will be determined mainly by the cavity pressure. Efforts were made on improving the theory. These included the wake pressure change by using $(\ell_c/c)^n$ in Equation (3.13) with n = 2 and 3, as well as the application of the wake thickness y_ϑ, similar to that used in the open wake model, but without success. It seems that more investigation will be worthwhile since the method is physically more reasonable and predicted the drag forces better than the infinite wake model. Finally, it must be mentioned for the limiting case as $\ell_c \to 0$, the two theories matched well.

4.3 CAVITY LENGTH vs. CAVITATION NUMBER

The cavity length as a function of cavitation number is one of the important features both in design and analysis work for high speed foils and propellers. Figures 4.11(a) through (e) show such data in comparison with some theoretical data. Except for the case of $\alpha = 4°$, the supercavitating foil theory predicts this relationship poorly. Both the experiment and theory are to blame for the discrepancy. For the short cavity cases, the theory seems to fail to represent the real flow pattern accurately, whereas for the long cavity cases, the water tunnel chokes so that the tunnel wall effect comes into the picture and causes an error in measurement.

As for the partially cavitating regime, the results made with the open wake model match well with the experimental data, whereas those of the double wake model have a substantial discrepancy. It must be mentioned again that success of any partially cavitating flow theory will require an accurate prediction of the cavitation number for the given cavity length.

5.0 CONCLUSION

As a preparatory phase for the cascade experiment to be conducted in the following phase, single-foil experiments were carried out. The blade profile shape of the foil selected here is that of Hydronautics 7607.02 supercavitating propeller at 50% radial station. It consisted of a modified Tulin two-term camber with a blunt trailing edge, which is considered to be a typical supercavitating foil profile shape. The foil was installed in the two-dimensional test section of the High Speed Water Tunnel at the California Institute of Technology and tested over a full range of cavitation numbers. Since it was found that there existed no appropriate nonlinear theories for comparison, the major effort after the experiment was directed towards the development of such theories. We have developed three nonlinear cavity-flow theories, one for supercavitating flows and two for partially cavitating flows. It is believed that these new nonlinear theories will provide tools for design and analysis of cavitating foils and propellers.

The success of the present experiments for the single foil has led us to design dummy foils which will form a cascade configuration for the following cascade experiments. Four dummy blades will be constructed for achieving the solidity of unity, but two dummy blades with the center blade may be tested for the solidity of 0.5. The drawing for the dummy blades has already been made for fabrication. The algorithm for HP9845 of controlling the downstream wall angle for the cascade experiment was also developed during the present work. Incidentally, this HP9845 was used even for the single foil experiments as an on-site data reduction system to help us reduce the experimental errors or discover any abnormalities during the work.

The conclusions drawn from the present preliminary work are summarized as follows:

1) The foil used for the present experiment could not maintain the leading edge cavitation at low incidence angles such as 2° or less. At 2° the cavity appeared both from the leading edge and trailing edge and by reducing it to 0°, the cavity stays at the trailing edge over a complete range of cavitation number.

2) Due to the flow pattern change from large to small incidence angles, the lift and drag force curve trends also changed. It seems that this was not predicted during the design work and it may be for this reason that the thrust coefficient of 7607.02 S/C propeller was overpredicted (see the paper of Peck (1977) for the comparison between the design value and experimental data). This propeller was designed under the assumption that the leading edge cavity would exist at local flow incidence angles of 2°, but the assumption seems incorrect.

3) For exactly the same reason as above, the overprediction of the thrust at the large J range with the off-design prediction method of Furuya (1978) may have arisen. We incorrectly used the force data which belonged to the leading edge cavity flows even for $\alpha_1 = 2°$. For such low incidence angles, we should have applied the data for base cavity flows. The forces there are much smaller than those of the S/C condition, as has been seen in the experimental results.

4) It is an extremely difficult task to determine theoretically at which incidence angle the cavity flow pattern changes from the leading edge cavity to base cavity, particularly for supercavitating foils having blunt trailing edges. This is one of the most important features for the design of supercavitating foils and propellers to determine their performance accurately and thus will require further investigation.

5) The supercavitating flow theory with the single spiral vortex model can accurately predict the force coefficients for the cases of cavity length larger than 1.5 chords, but underpredicts for shorter cavity cases.

6) The partially cavitating flow theory with the double wake model failed to predict the right cavitation number for the specified cavity length, thus substantially underpredicted the force coefficients.

7) The partially cavitating flow theory with the open wake model could fit the lift curves with the experimental data by adjusting the turbulent mixing wake thickness. The wake thickness was determined as a function of α for the present cases but needs justification for its applicability to other foil profiles.

8) Both partially cavitating flow theories predicted the drag forces with poor accuracy.

9) The prediction accuracy of all the theories developed here degrades as soon as the cavity collapses near the trailing edge of the foil both for the supercavitating and partial cavitating conditions. It seems that highly turbulent flow phenomena near the cavity collapse will need a better flow modeling for mathematical formulation.

10) The analytical prediction capability for the partial cavity length is important for the high speed propeller analysis. The theory with the infinite wake model showed a promising feature for this purpose but its universal application still remains to be seen.

6.0 REFERENCES

Baker, E.S., 1972, Analytical prediction of wall effects on fully cavitating lifting foils, using nonlinear theory. *NSRDC Report 3638; November.*

Barker, S.T. and Ward, T.M., 1976, Experiments on two and three dimensional cavitating hydrofoil models with and without flaps. *IAUOIT Report HSWT-1020 of the California Institute of Technology.*

Bohn, J. and Altman, R., 1976, Two supercavitating propeller designs for hydrofoil ships, *Hydronautics Technical Report 7607.01-1.*

Furuya, O., 1978, Part I: Calculations of the off-design performance for hydronautics' S/C Propeller, Part II: Theory improvement for computer code "SCSCREW". *Tetra Tech Report TC-3913 and 3233.*

Furuya, O., 1975, Exact supercavitating cascade theory. *Journal of Fluid Engineering, ASME. Vol. 97, December, 419-429.*

Furuya, O., 1976, Development of an off-design predictive method for supercavitating propeller performance. *Tetra Tech Report TC-676.*

Furuya, O. and Maekawa, S., 1979, Partially cavitating cascade theories and their application to cavitating propeller flows. *Tetra Tech Report TC-3934-01.*

Furuya, O., 1980, Nonlinear theory for partially cavitating cascade flows. *10th Symposium of IAHR, Tokyo, Japan, 221-241.*

Kermeen, R.W., 1956, Water tunnel tests of NACA 4412 and Walchner profile 7 hydrofoils in noncavitating and cavitating flows. *Hydrodynamics Lab. Report No. 47.5 of the California Institute of Technology.*

Knapp, R.T., Levy, J., O'Neill, J.P. and Brown, F.B., 1948, The hydrodynamics laboratory of the California Institute of Technology. *Transactions of the ASME, Vol. 70.*

Larock, R.E. and Street, R.L., 1965, A Riemann-Hilbert problem for nonlinear, fully cavitating flow. *Journal of Ship Research, Vol. 9, 173-178.*

Larock, R.E. and Street, R.L., 1968, Cambered bodies in cavitating flow - a nonlinear analysis and design procedure. *Journal of Ship Research, Vol. 12, 1-10.*

Peck, J.G., 1977, Cavitation performance characteristics of supercavitating propellers 4698 and 4999. *DTNSRDC Ship Performance Department, Department Report SPD-[illegible]-01, December.*

Tulin, M.P., 1964, Supercavitating flows - small perturbation theory. *Journal of Ship Research, Vol. [illegible], No. [illegible].*

Wade, R.B. and Acosta, A.J., 1966, Experimental observations on the flow past a plano-convex hydrofoil. *Transactions of the ASME, J. of Basic Engineering, Series D, Vol. [illegible], p. [illegible].*

Wade, R.B. and Acosta, A.J., 1967, Investigation of cavitating cascade. *ASME, J. of Basic Engineering, December, [illegible].*

Ward, T.M., 1976, The hydrodynamics laboratory at the California Institute of Technology--1976. *Transactions of the ASME, J. of Fluids Engineering, December. [illegible].*

Wu, T.Y., Whitney, A.K. and Brennen, C., 1971, Cavity flow wall effects and correction rules. *J. of Fluid Mechanics, Vol. 49, 223-256.*

Wu, T.K. and Wang, D.P., 1964, A wake model for free-streamline flow theory. Part II: Cavity flows past obstacles of arbitrary profile. *J. of Fluid Mechanics, 19, 65-83.*

TABLE 2.1

MODEL BLADE OFF-SET POINTS
(Hydronautics 7607.02 S/C Propeller at 50% Radial Station)

STATION		OFFSET INCHES		TOTAL THICKNESS	
Percent Chord	Distance from L.E.	Upper (Back)	Lower Face	Inches	Percent
0	0	0	0	0	0
5	.160	.023	-.009	.032	1.0
10	.320	.039	-.016	.055	1.7
15	.480	.051	-.023	.074	2.3
20	.640	.060	-.029	.089	2.8
25	.800	.068	-.036	.104	3.3
30	.960	.075	-.044	.119	3.7
35	1.120	.082	-.052	.134	4.2
40	1.280	.088	-.060	.148	4.6
45	1.440	.093	-.068	.161	5.0
50	1.600	.098	-.077	.175	5.5
55	1.760	.103	-.086	.189	5.9
60	1.920	.107	-.096	.203	6.3
65	2.080	.110	-.107	.217	6.8
70	2.240	.114	-.117	.231	7.2
75	2.400	.116	-.129	.245	7.7
80	2.560	.119	-.140	.259	8.1
85	2.720	.120	-.153	.273	8.5
90	2.880	.122	-.167	.289	9.0
95	3.040	.122	-.183	.305	9.5
100	3.200	.121	-.202	.323	10.1

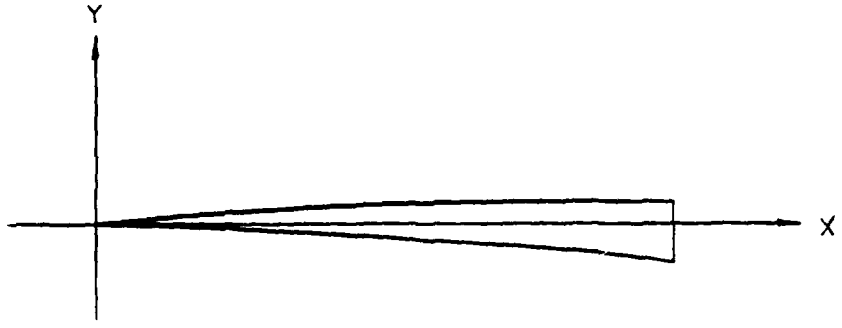

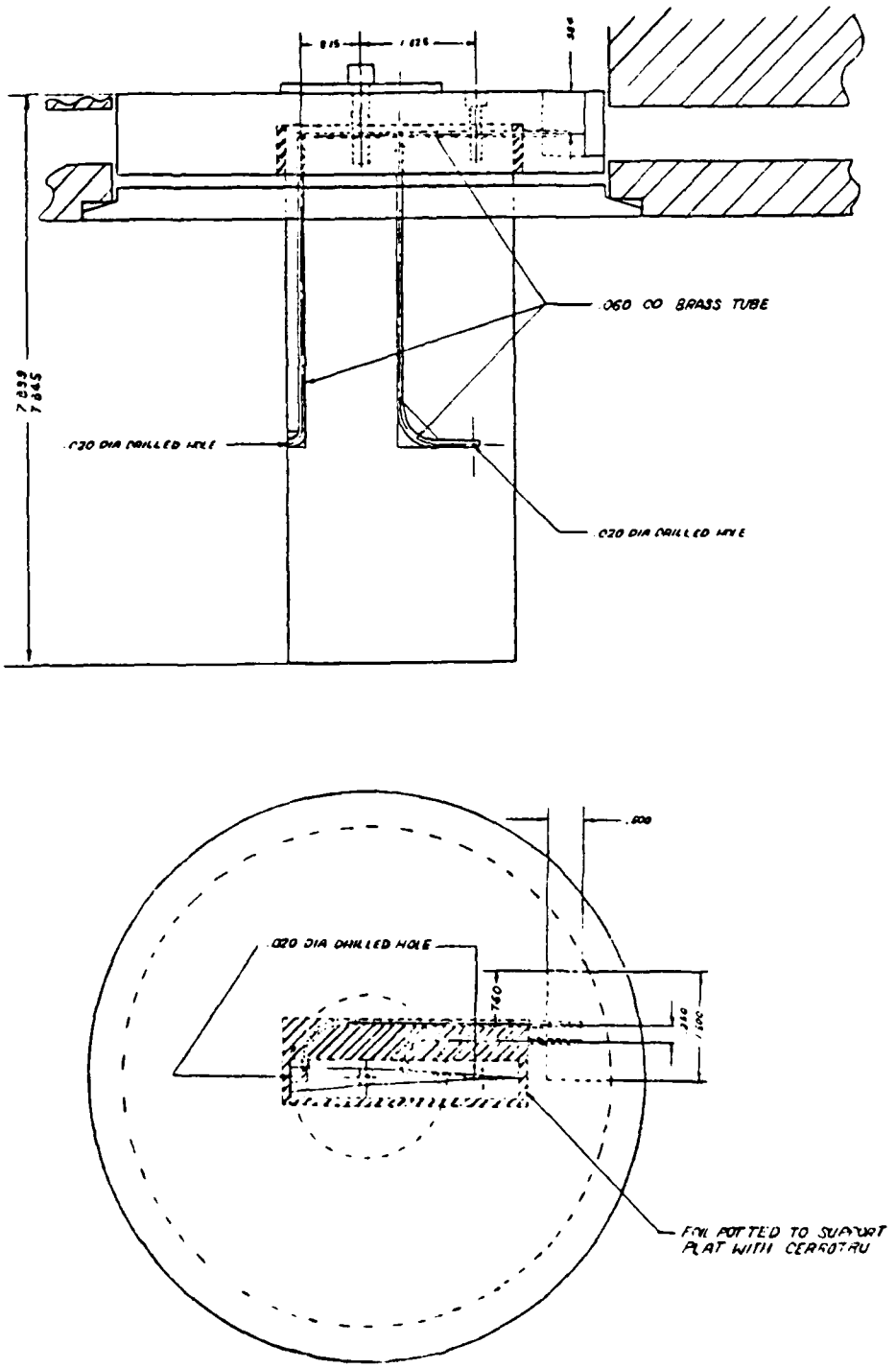

FIGURE 2.1
BLADE SET-UP TO THE TUNNEL WALL

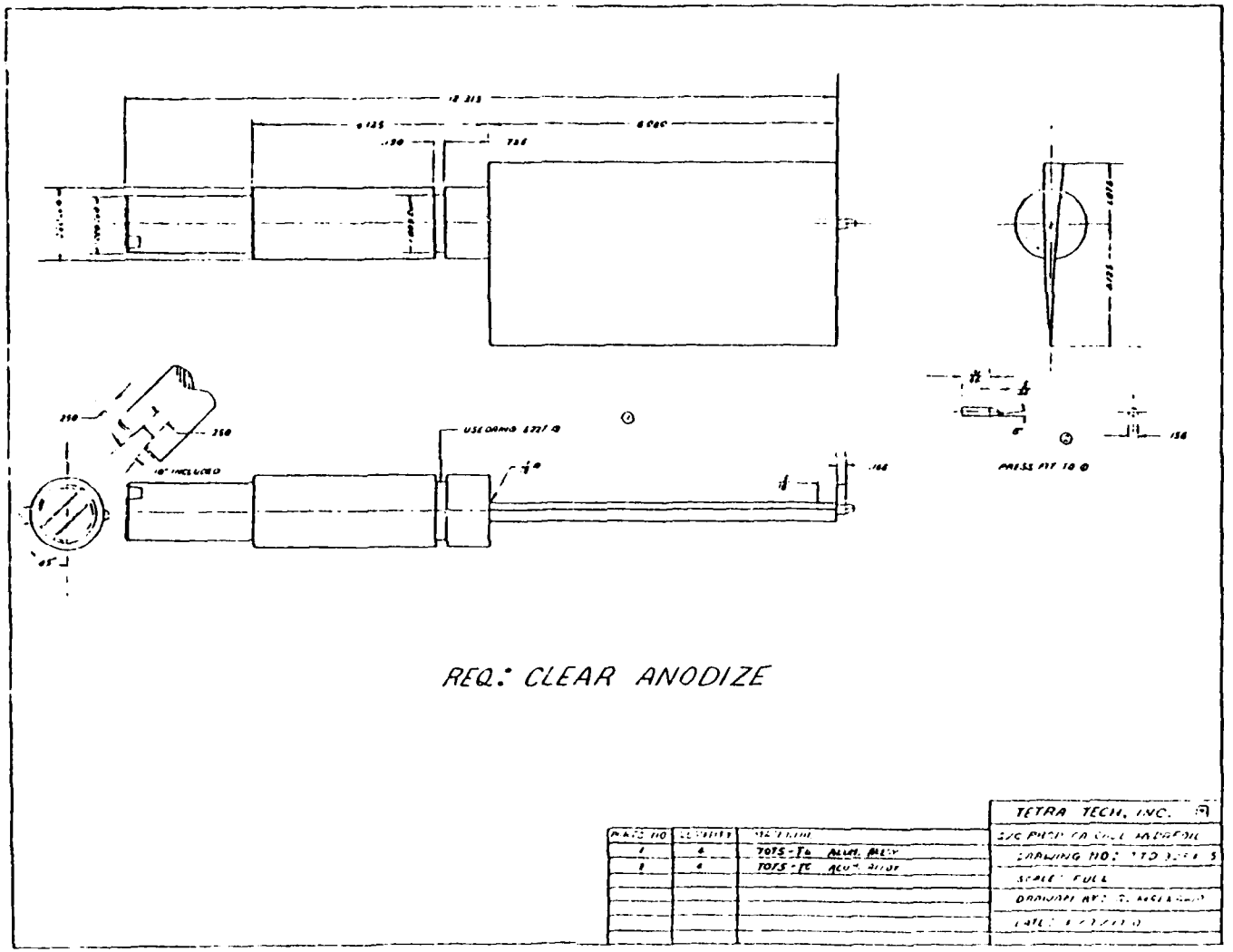

FIGURE 2.2
DUMMY BLADES FOR CASCADE EXPERIMENTS

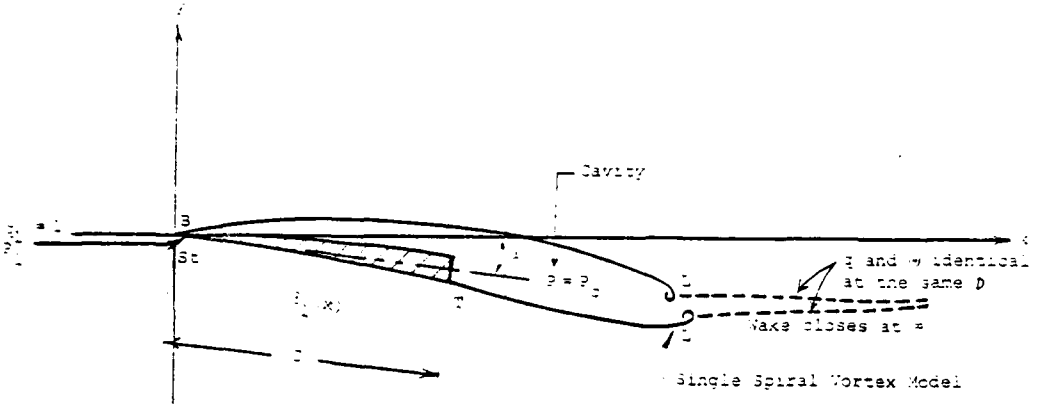

FIGURE 3.1
FLOW CONFIGURATION FOR S/C FOIL

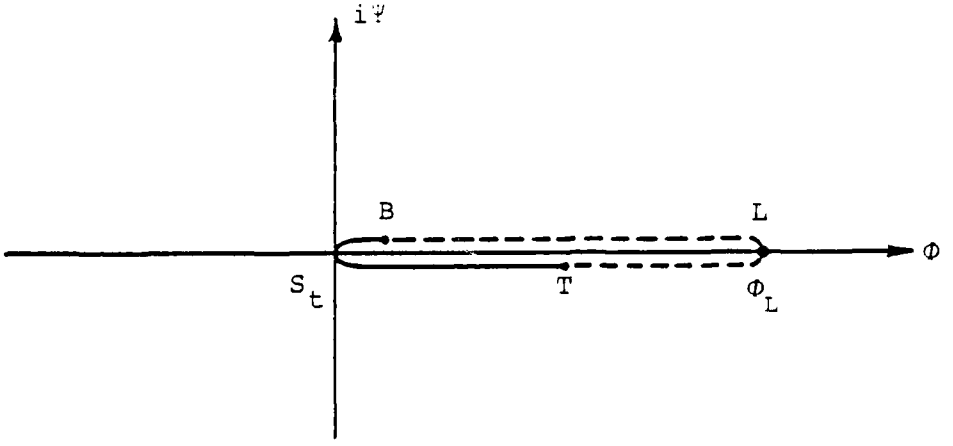

FIGURE 3.2
POTENTIAL PLANE

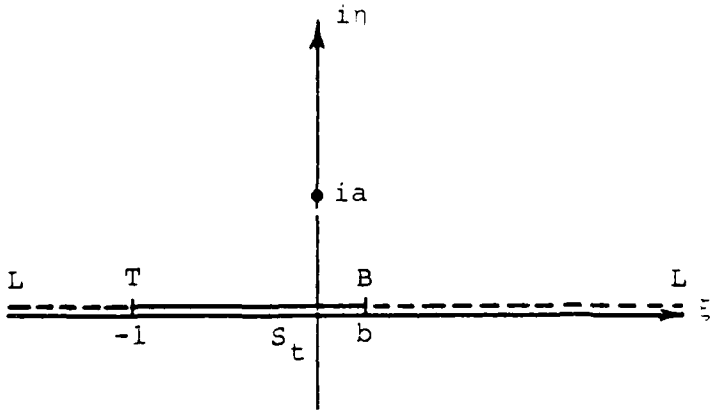

FIGURE 3.3
TRANSFORM PLANE

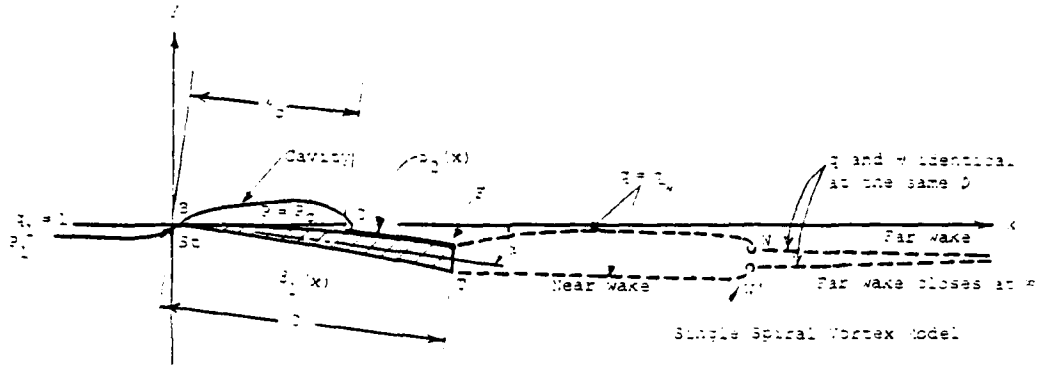

FIGURE 3.4
FLOW CONFIGURATION OF DOUBLE WAKE
MODEL FOR PARTIALLY CAVITATING FOIL

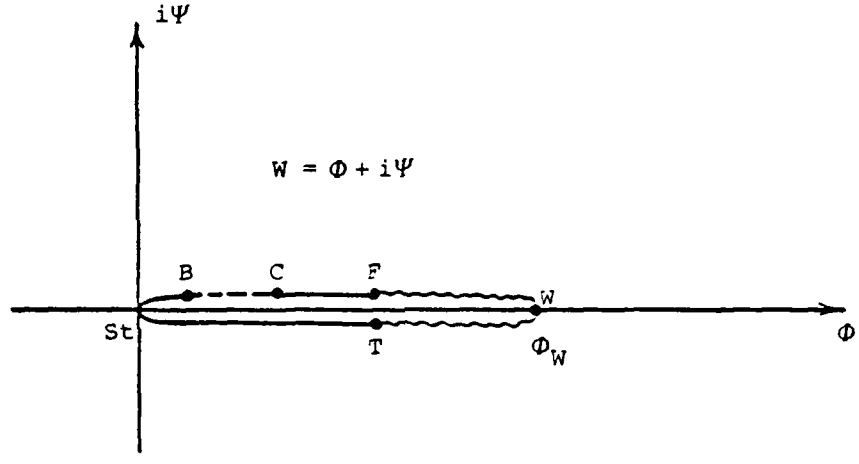

FIGURE 3.5
POTENTIAL PLANE

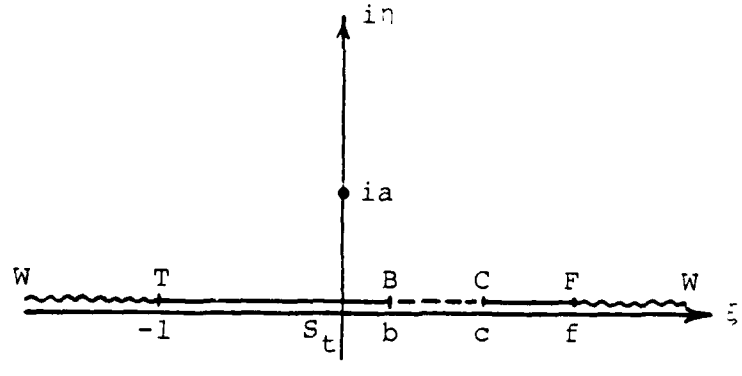

FIGURE 3.6
TRANSFORM PLANE

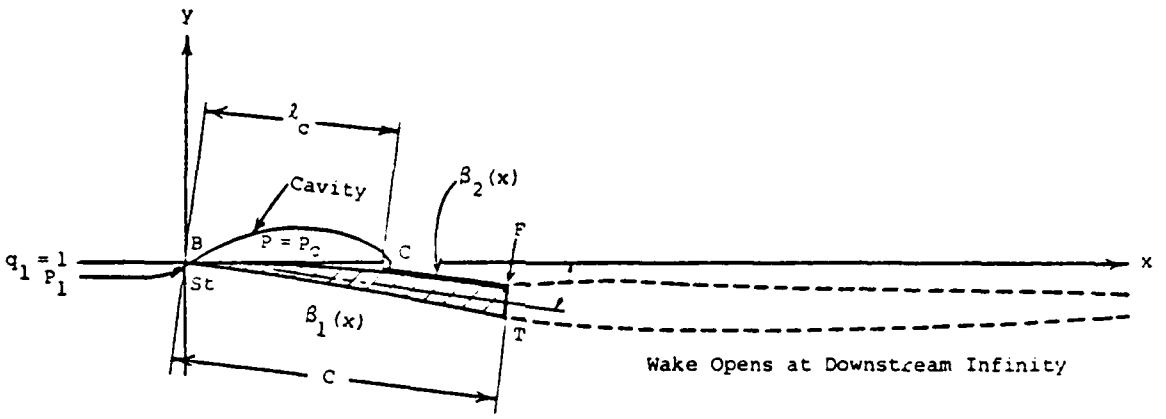

FIGURE 3.7
FLOW CONFIGURATION OF OPEN WAKE MODEL
FOR PARTIALLY CAVITATING FOIL

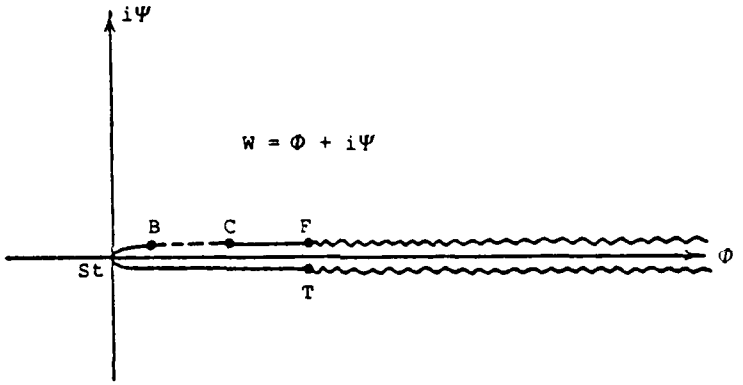

FIGURE 3.8
POTENTIAL PLANE

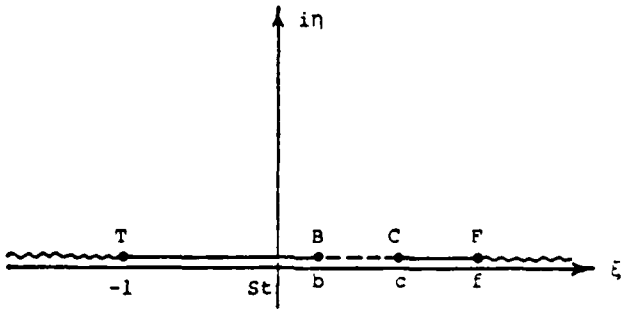

FIGURE 3.9
TRANSFORM PLANE

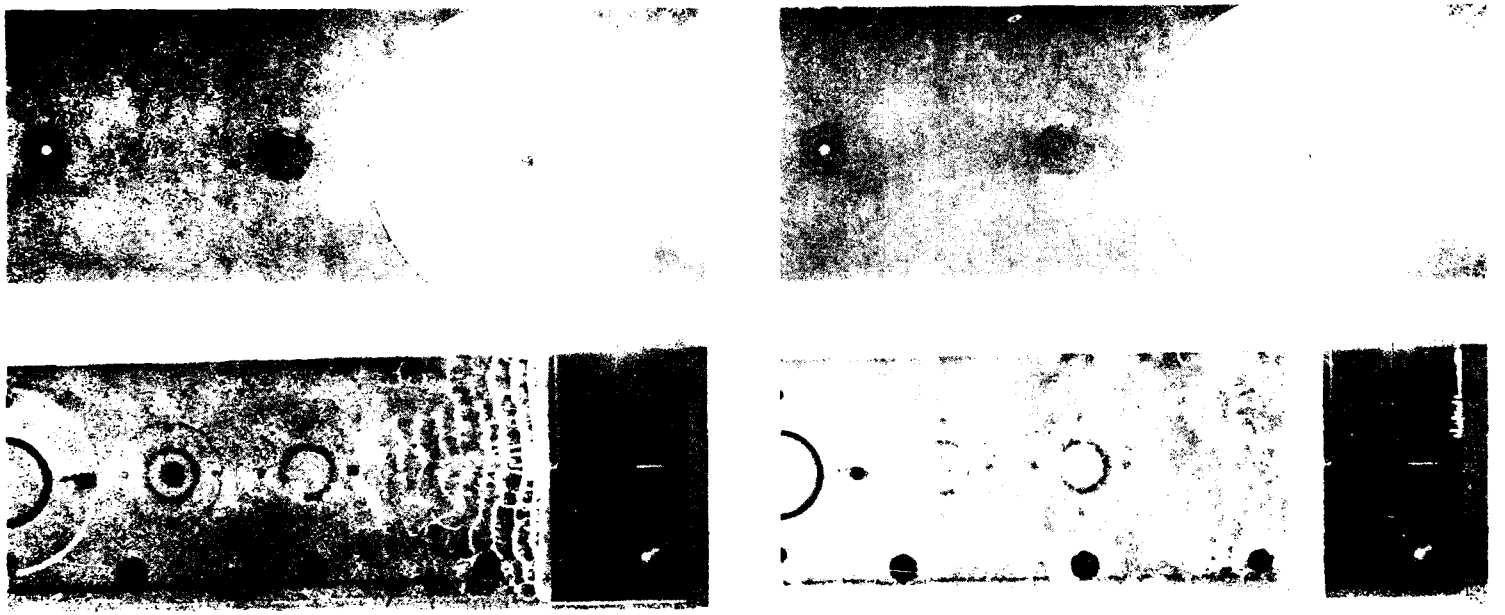

(a) σ = .99

(b) σ = .36

FIGURE 4.1 SIMULTANEOUS VIEWS FROM TOP AND SIDE FOR INCIDENCE ANGLE α = 0°

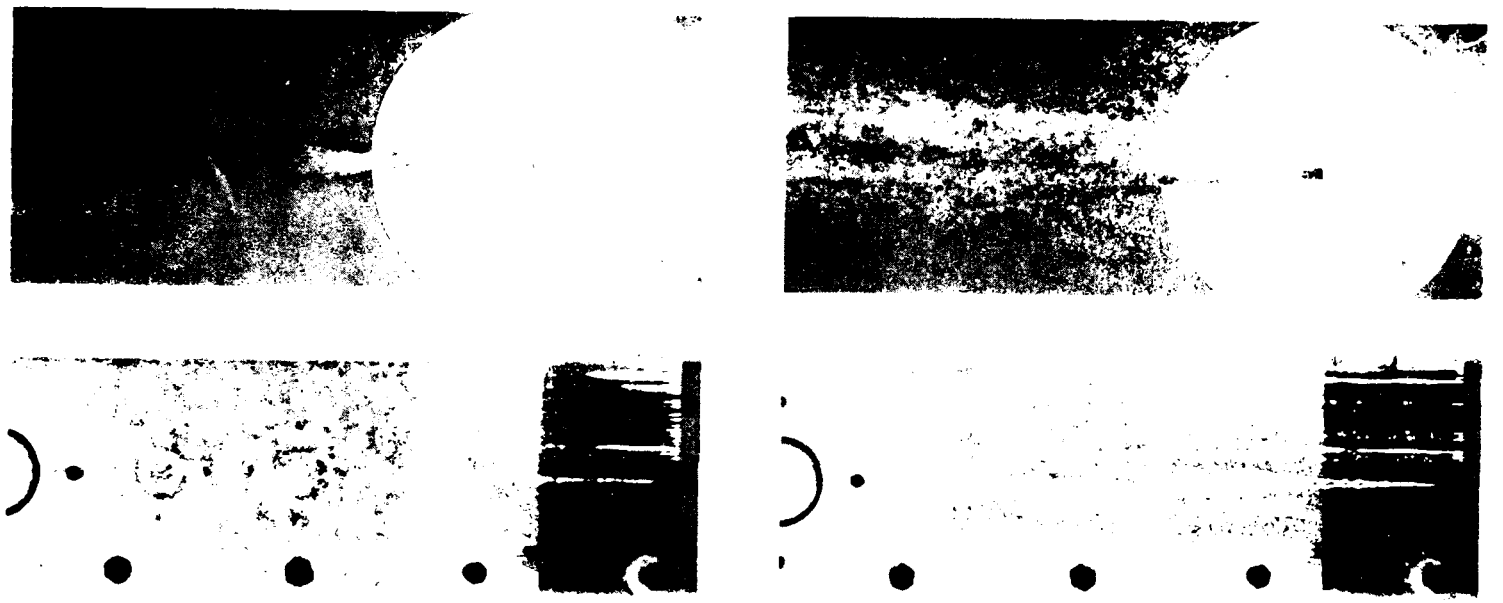

(c) σ = .18

(d) σ = .14

FIGURE 4.1 CONTINUED

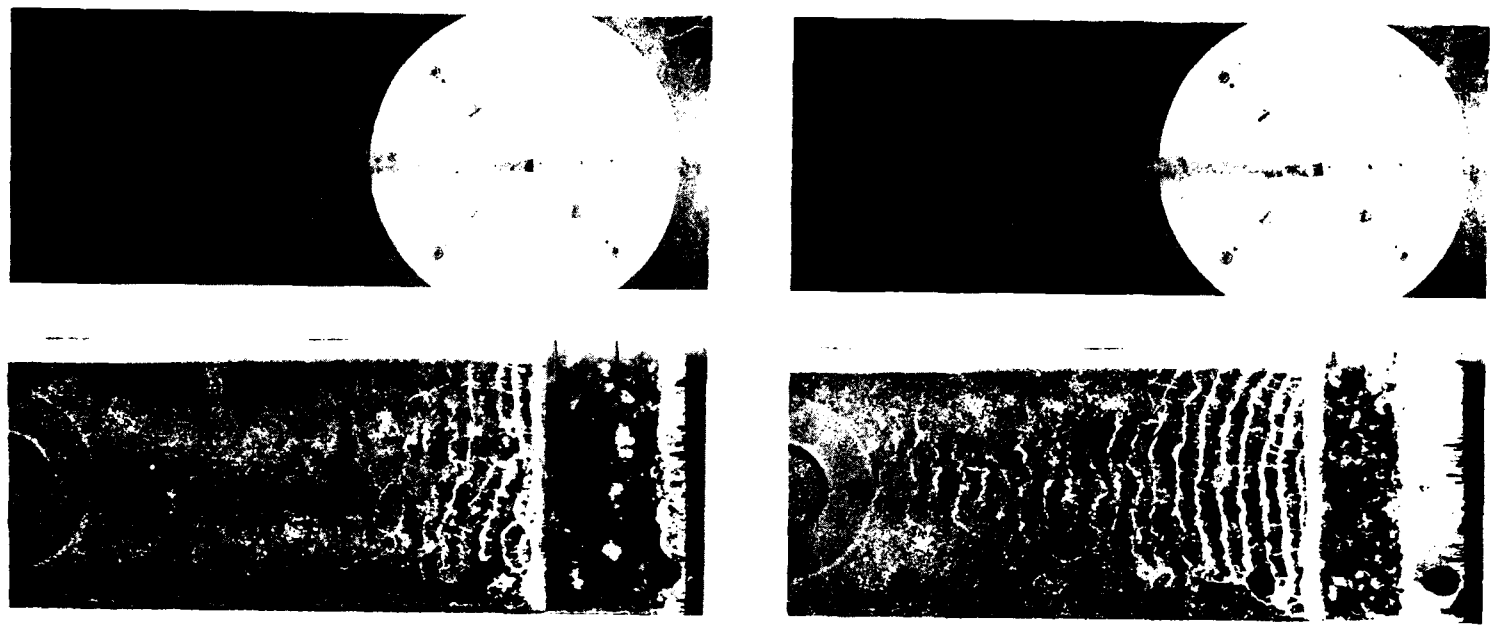

(a) σ = .70

(b) σ = .61

FIGURE 4.2 SIMULTANEOUS VIEWS FROM TOP AND SIDE FOR INCIDENCE ANGLE α = 2°

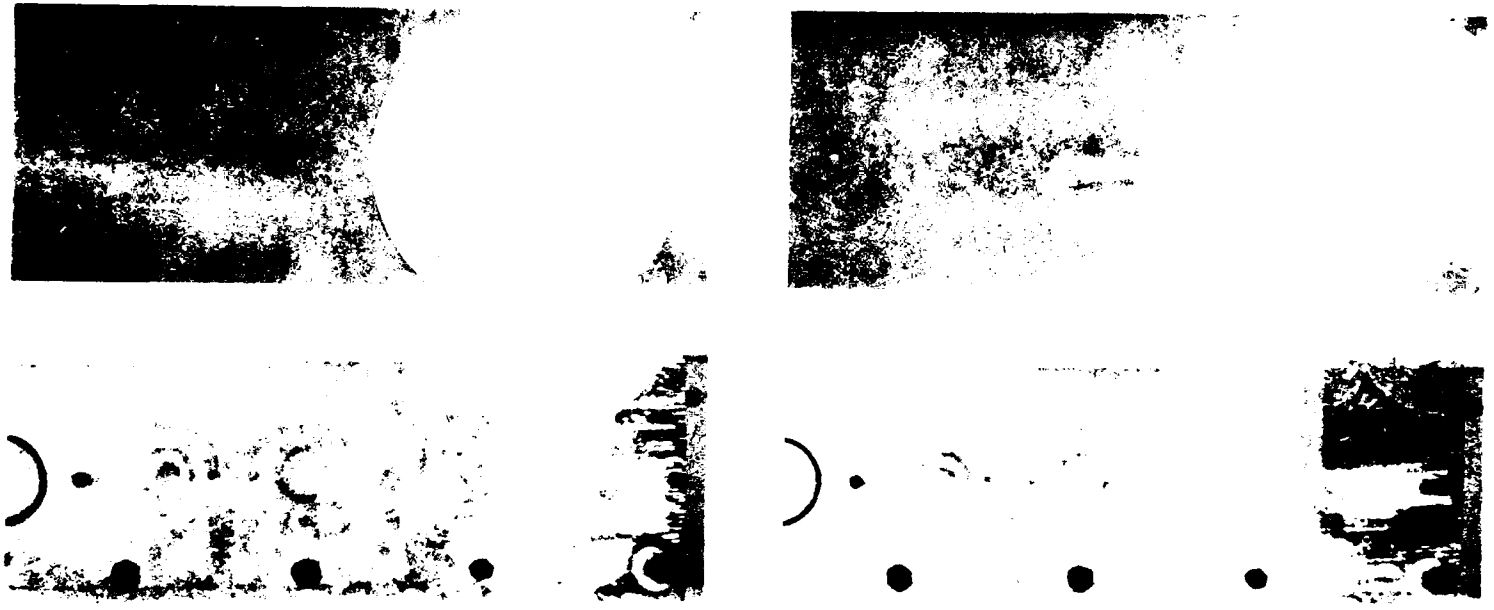

(c) σ = .35

(d) σ = .22

FIGURE 4.2 CONTINUED

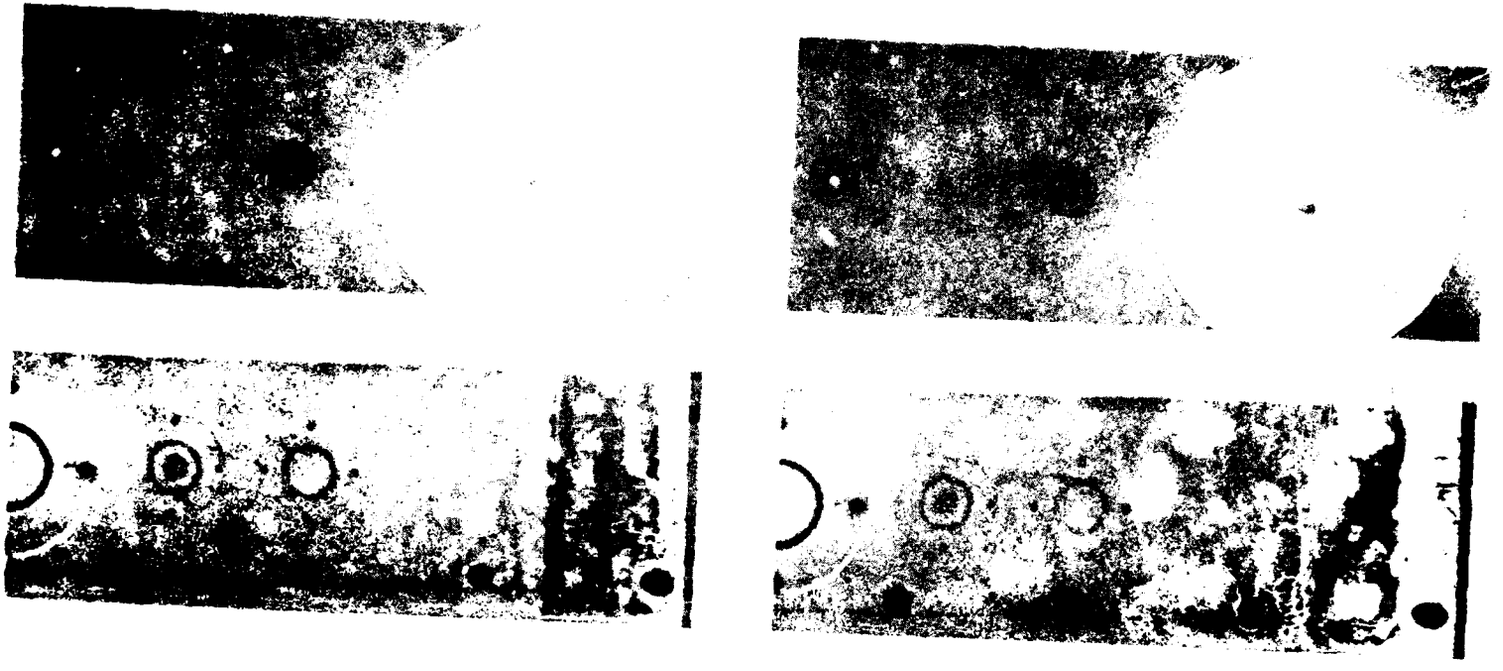

(a) $\sigma = 1.67$

(b) $\sigma = .91$

FIGURE 4.3 SIMULTANEOUS VIEWS FROM TOP AND SIDE FOR INCIDENCE ANGLE $\alpha = 4°$

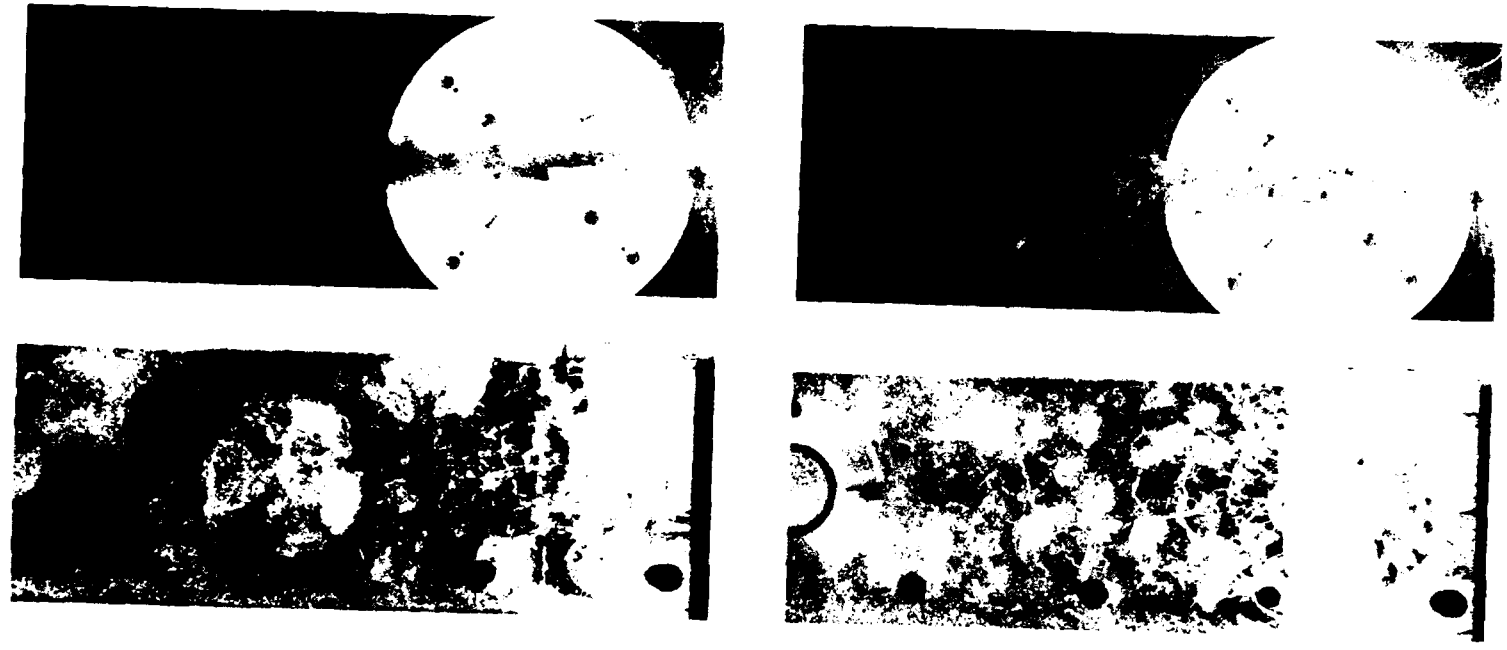

(c) σ = .75

(d) σ = .48

FIGURE 4.3 CONTINUED

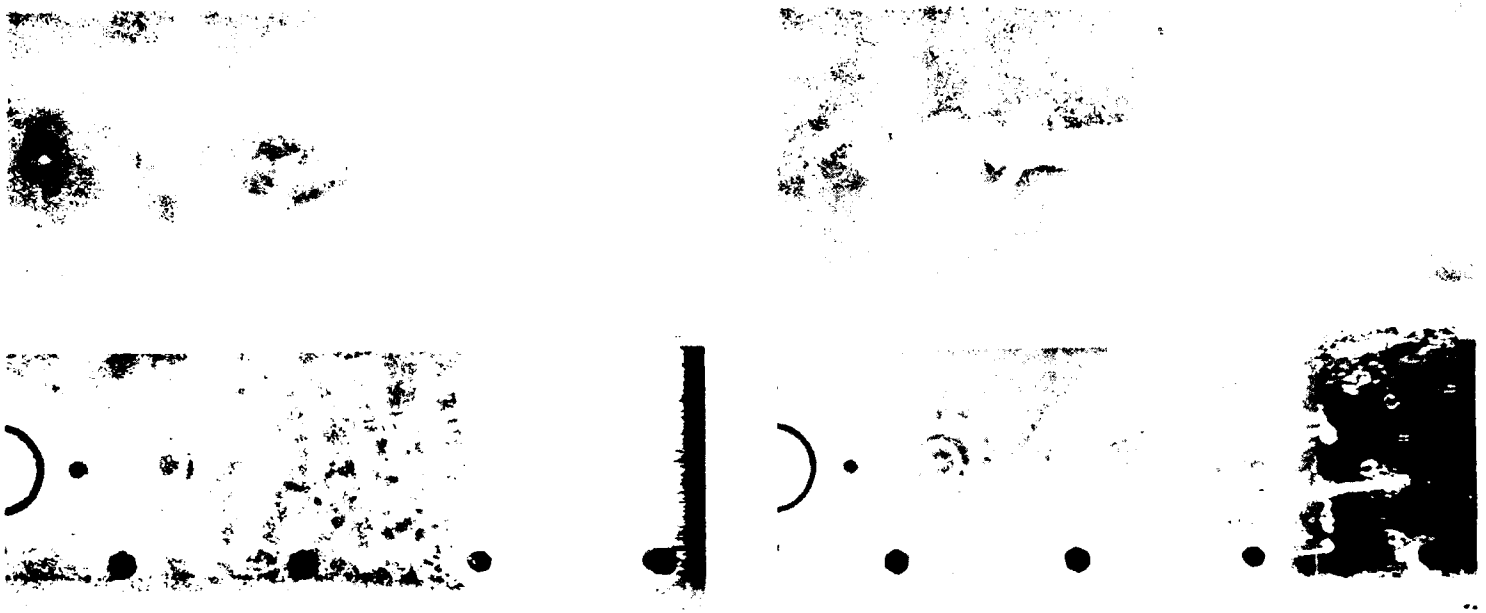

(e) σ = .38

(f) σ = .27

FIGURE 4.3 CONTINUED

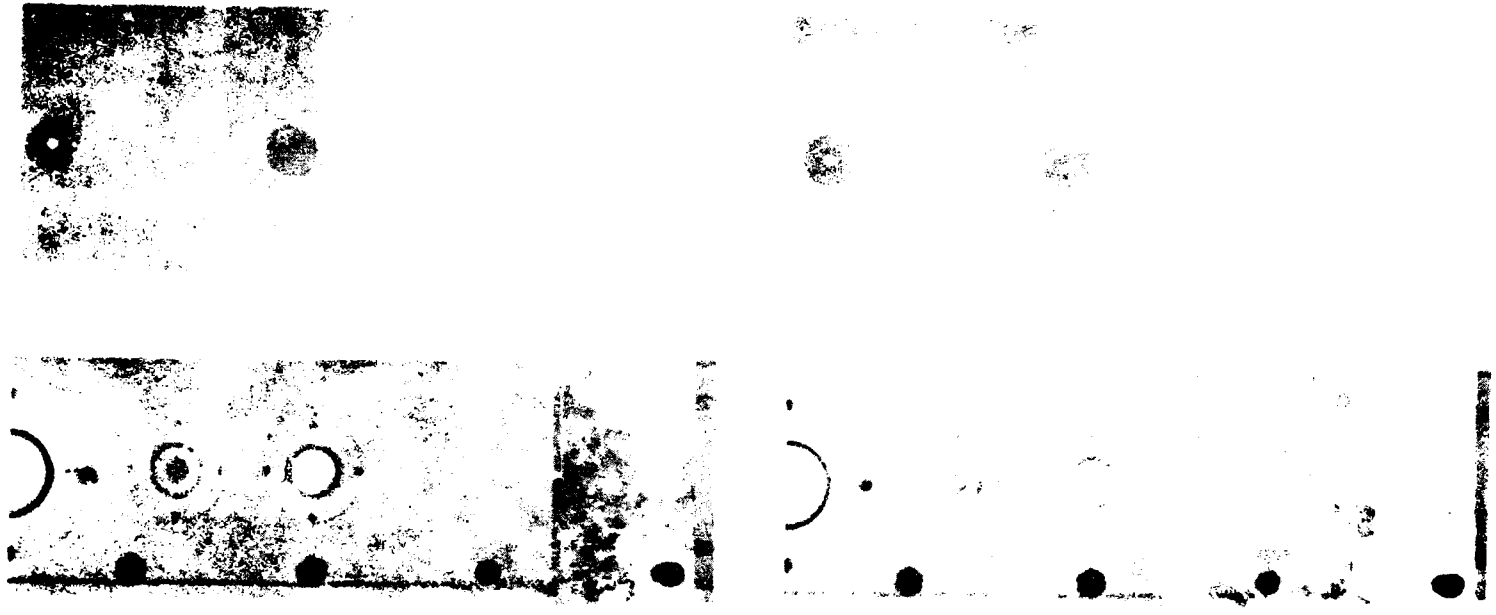

(a) $\sigma = 1.86$

(b) $\sigma = 1.07$

FIGURE 4.4 SIMULTANEOUS VIEWS FROM TOP AND SIDE FOR INCIDENCE ANGLE $\alpha = 6°$

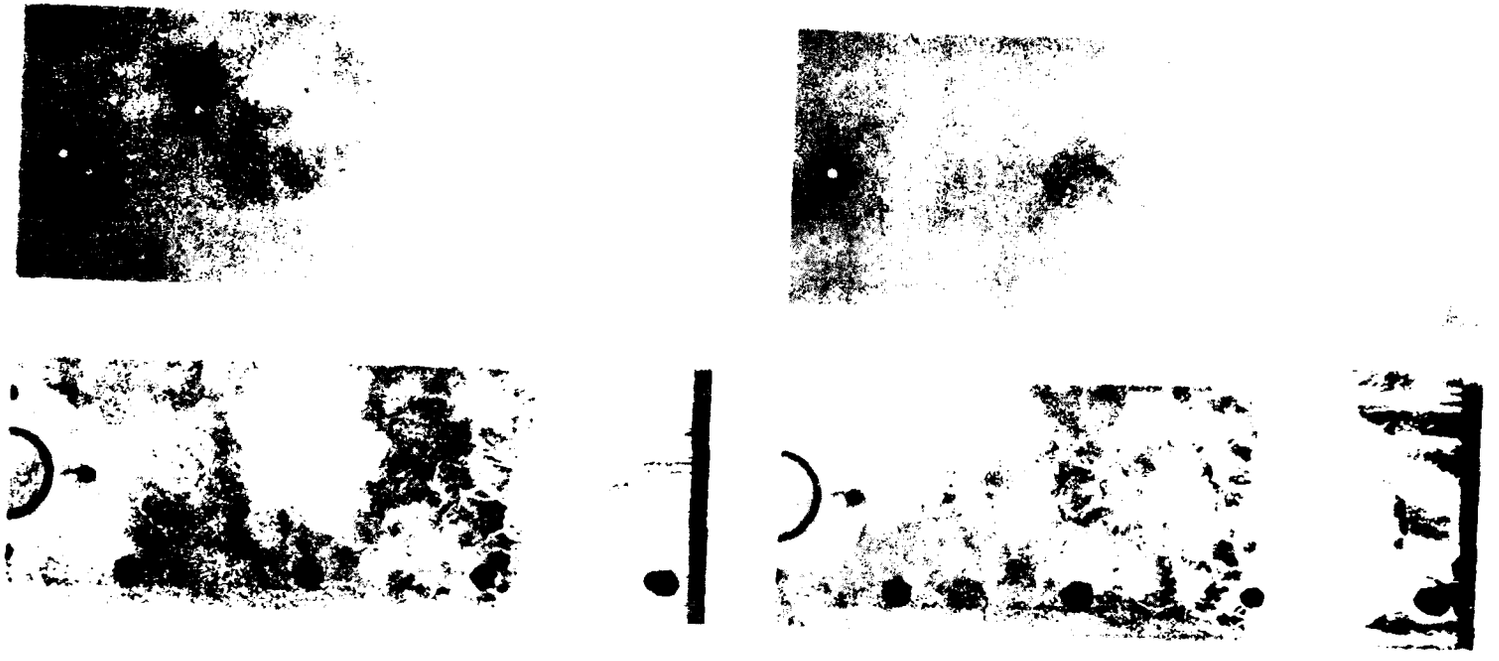

(c) σ = .88

(d) σ = .52

FIGURE 4.4 CONTINUED

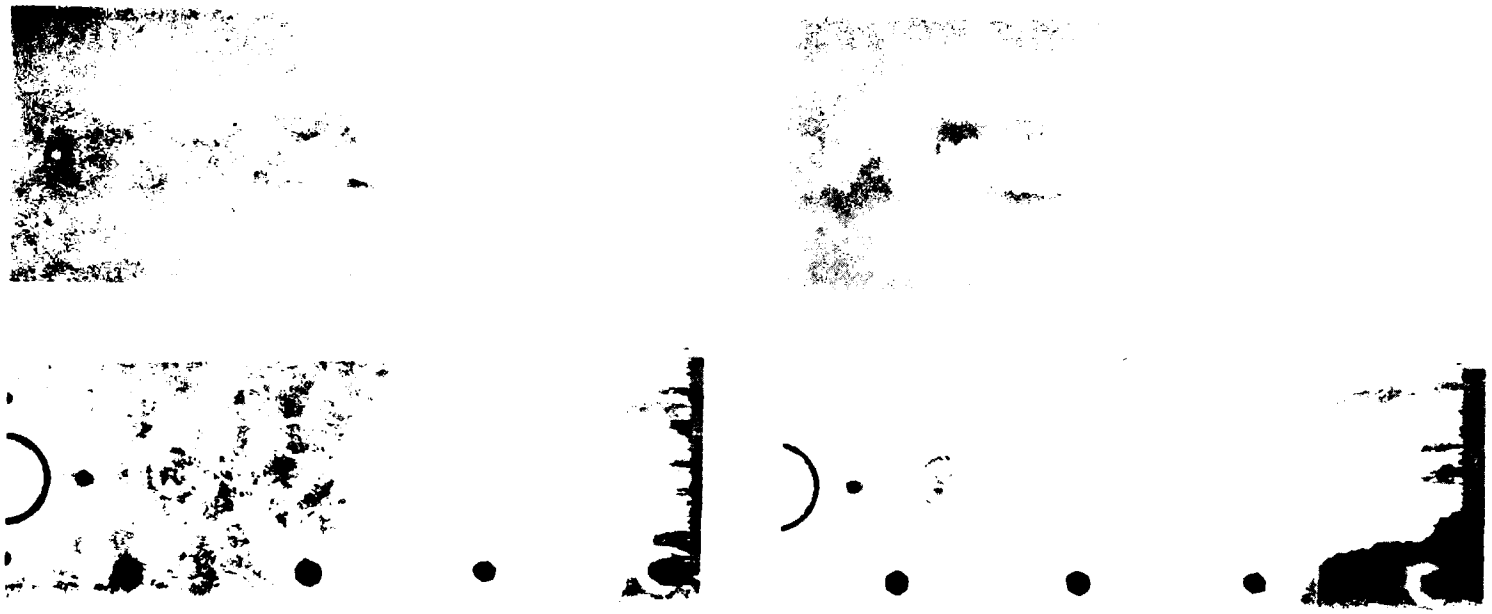

(e) σ = .33

(f) σ = .28

FIGURE 4.4 CONTINUED

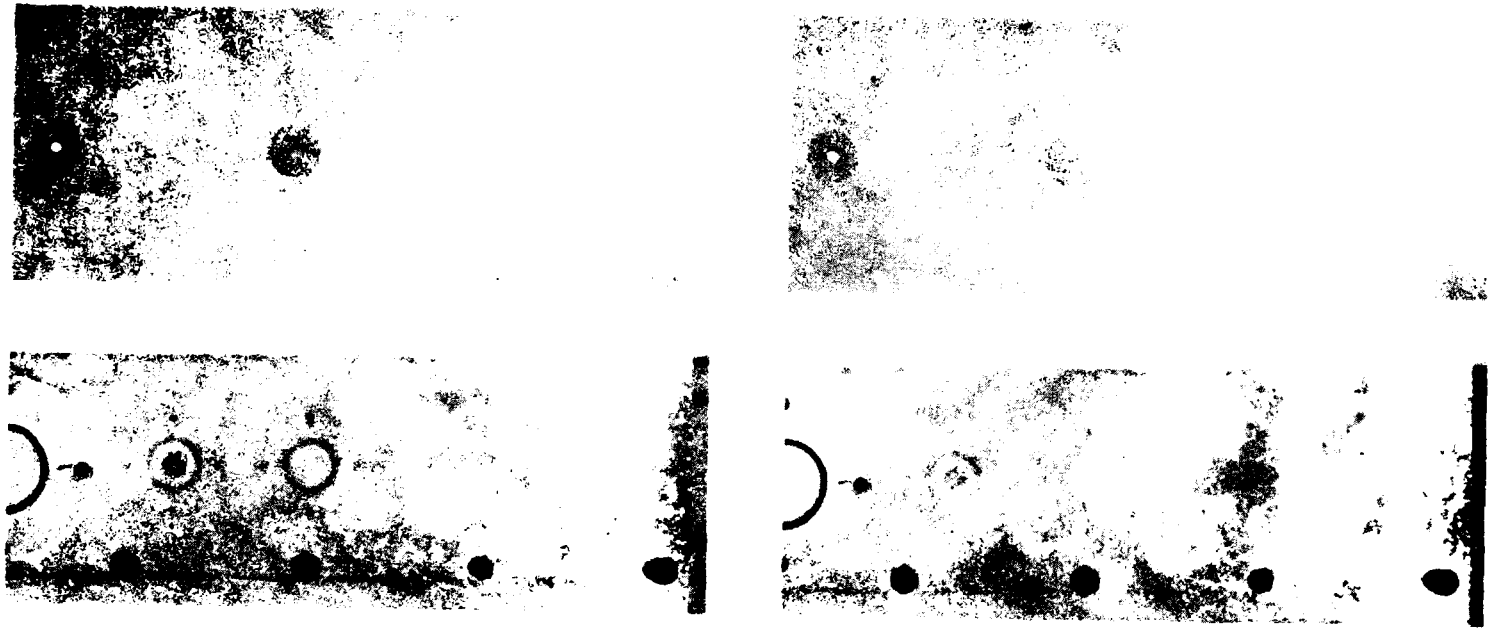

(a) σ = 1.76

(b) σ = 1.06

FIGURE 4.5 SIMULTANEOUS VIEWS FROM TOP AND SIDE FOR INCIDENCE ANGLE α = 10°

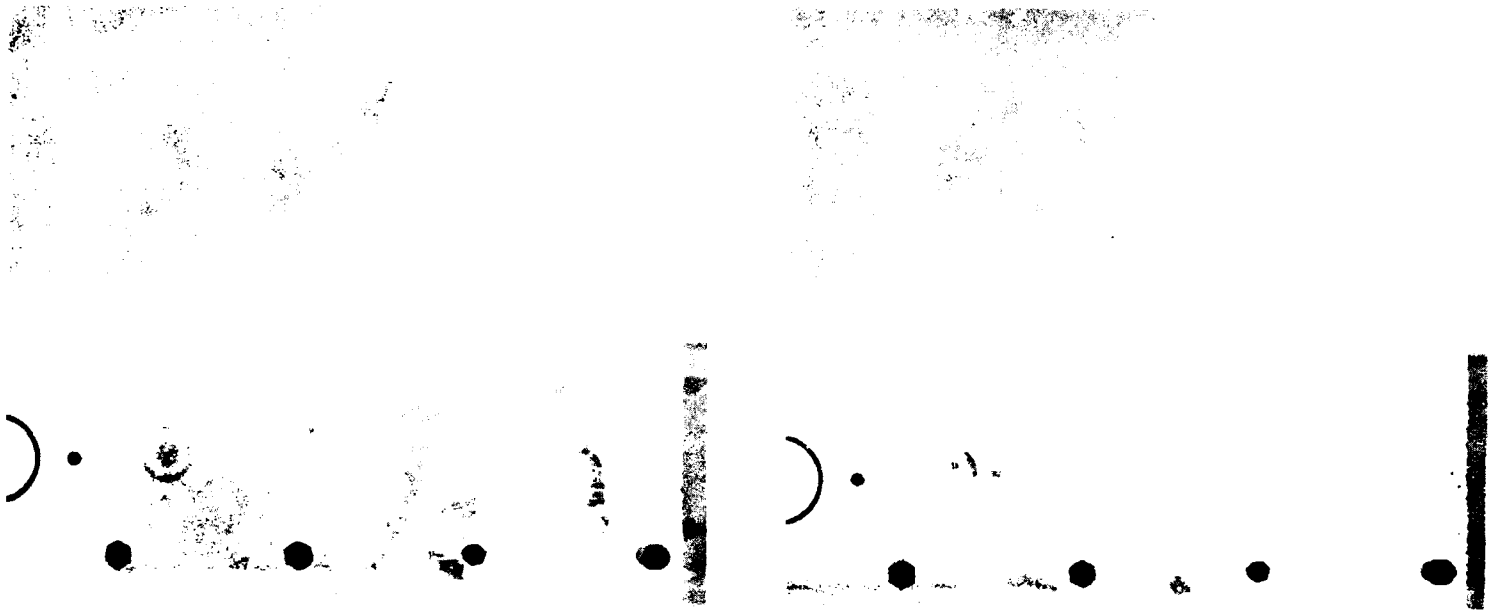

(c) σ = .88

(d) σ = .54

FIGURE 4.5 CONTINUED

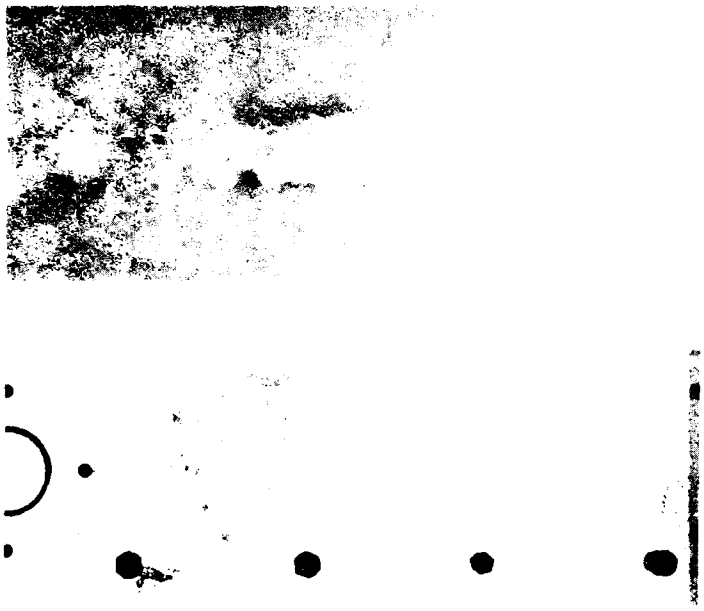

(e) σ = .42

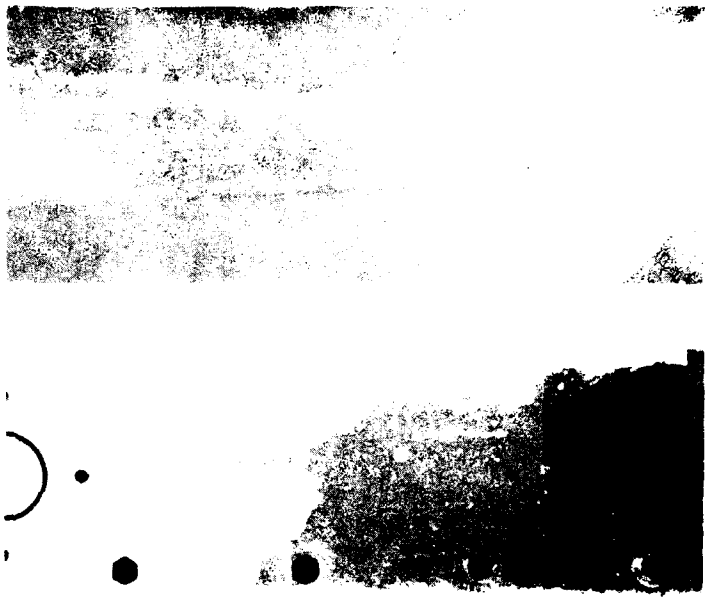

(f) σ = .39

FIGURE 4.5 CONTINUED

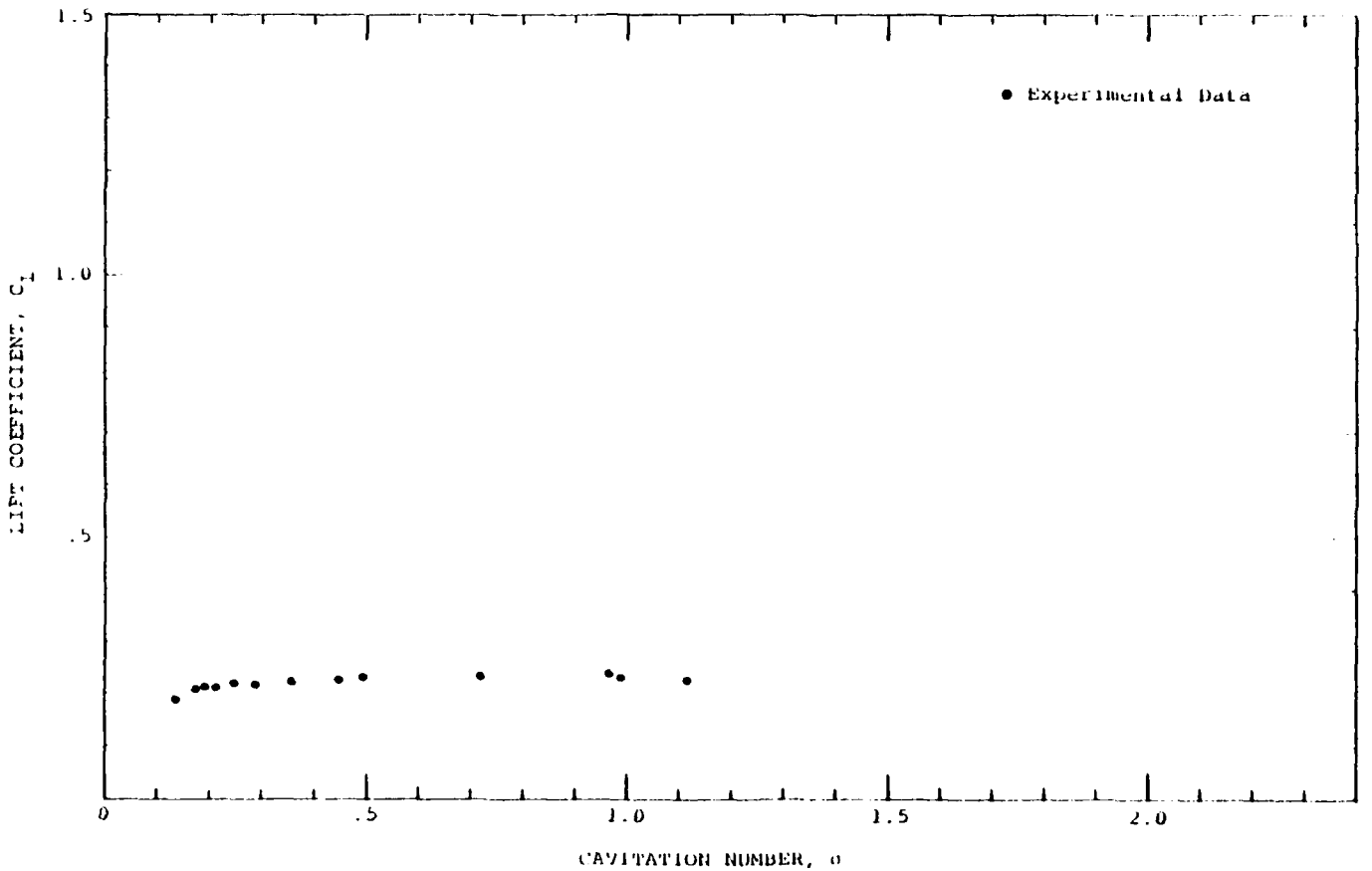

(a) $\alpha = 0°$

FIGURE 4.6
LIFT COEFFICIENT AS A FUNCTION OF CAVITATION NUMBER

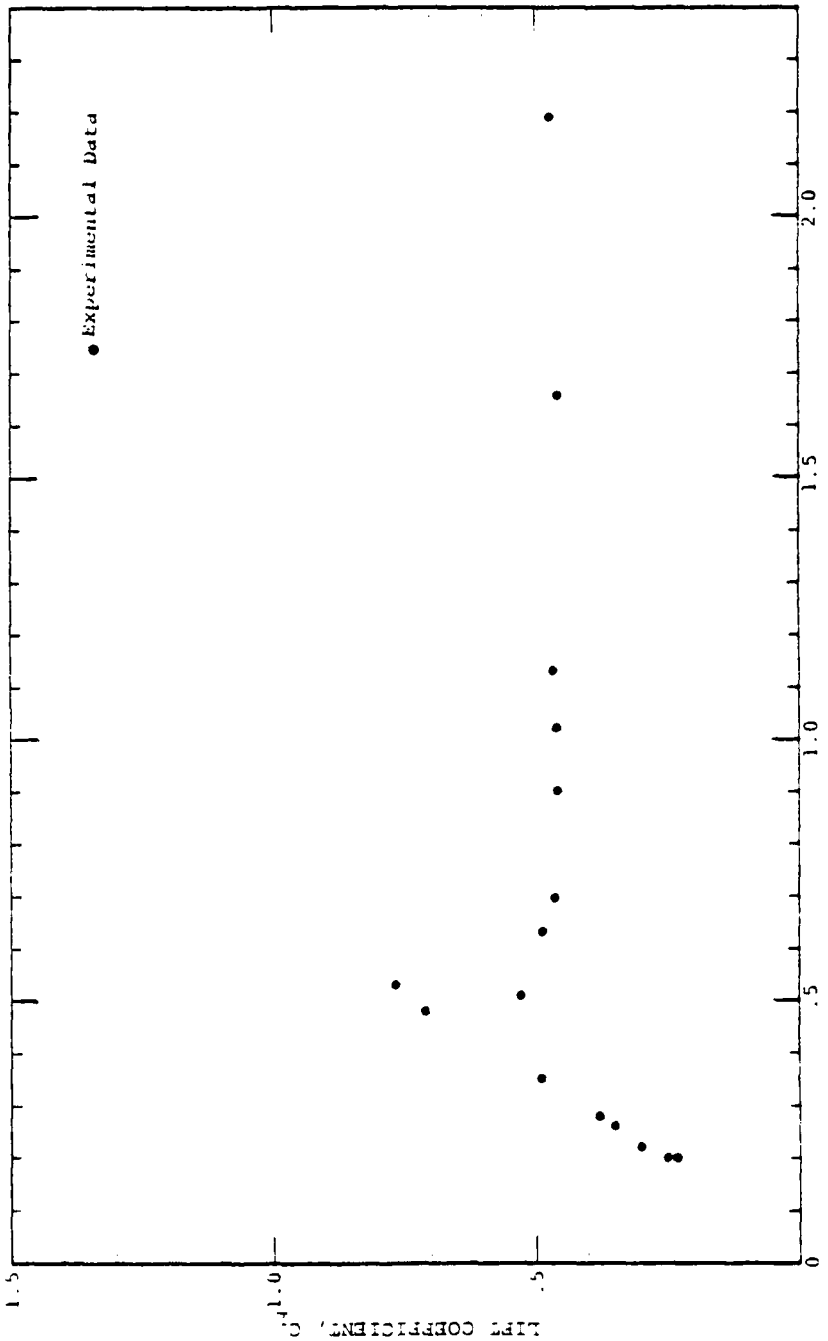

(b) $\alpha = 2°$

FIGURE 4.6 CONTINUED

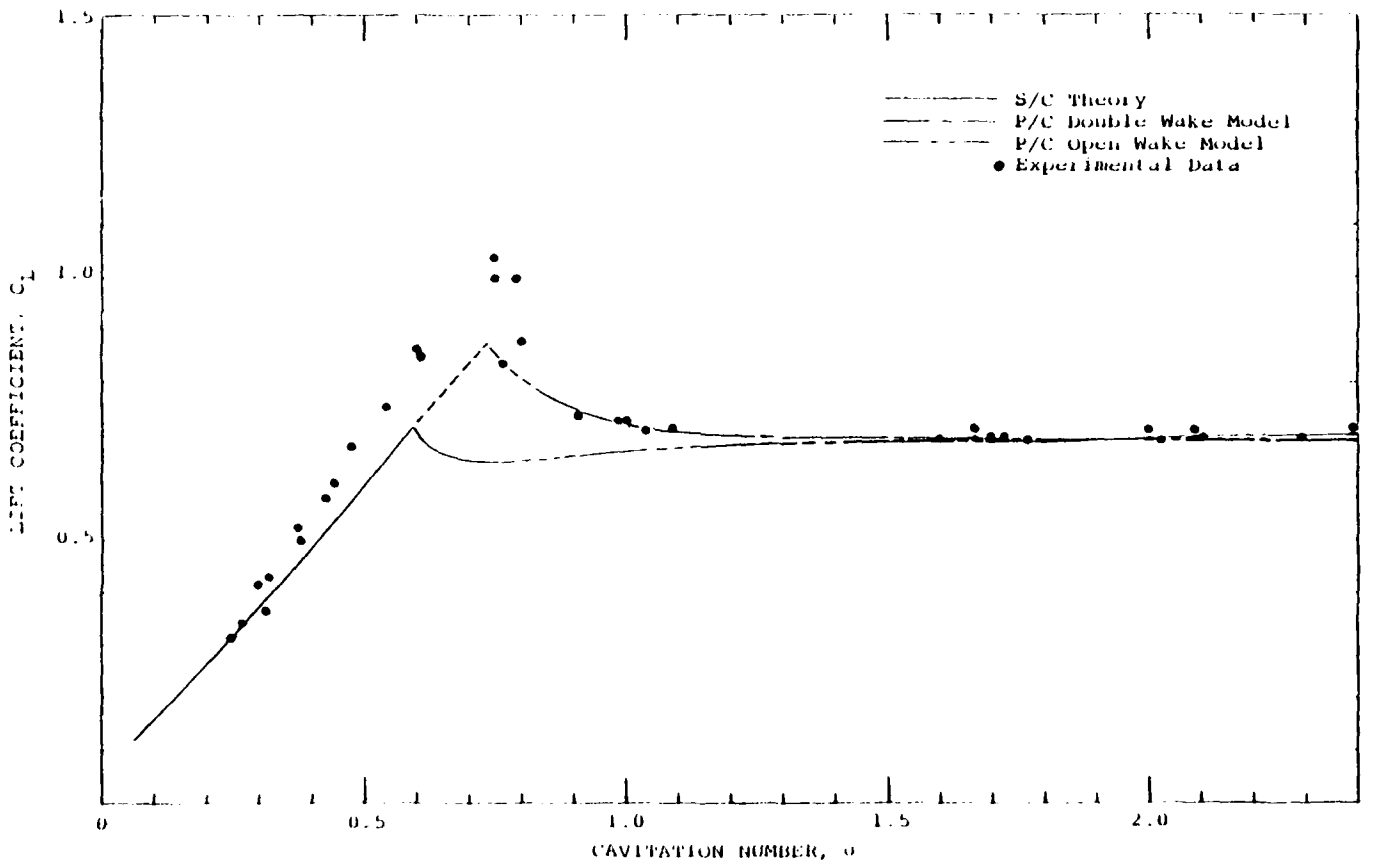

(c) $\alpha = 4°$

FIGURE 4.6 CONTINUED

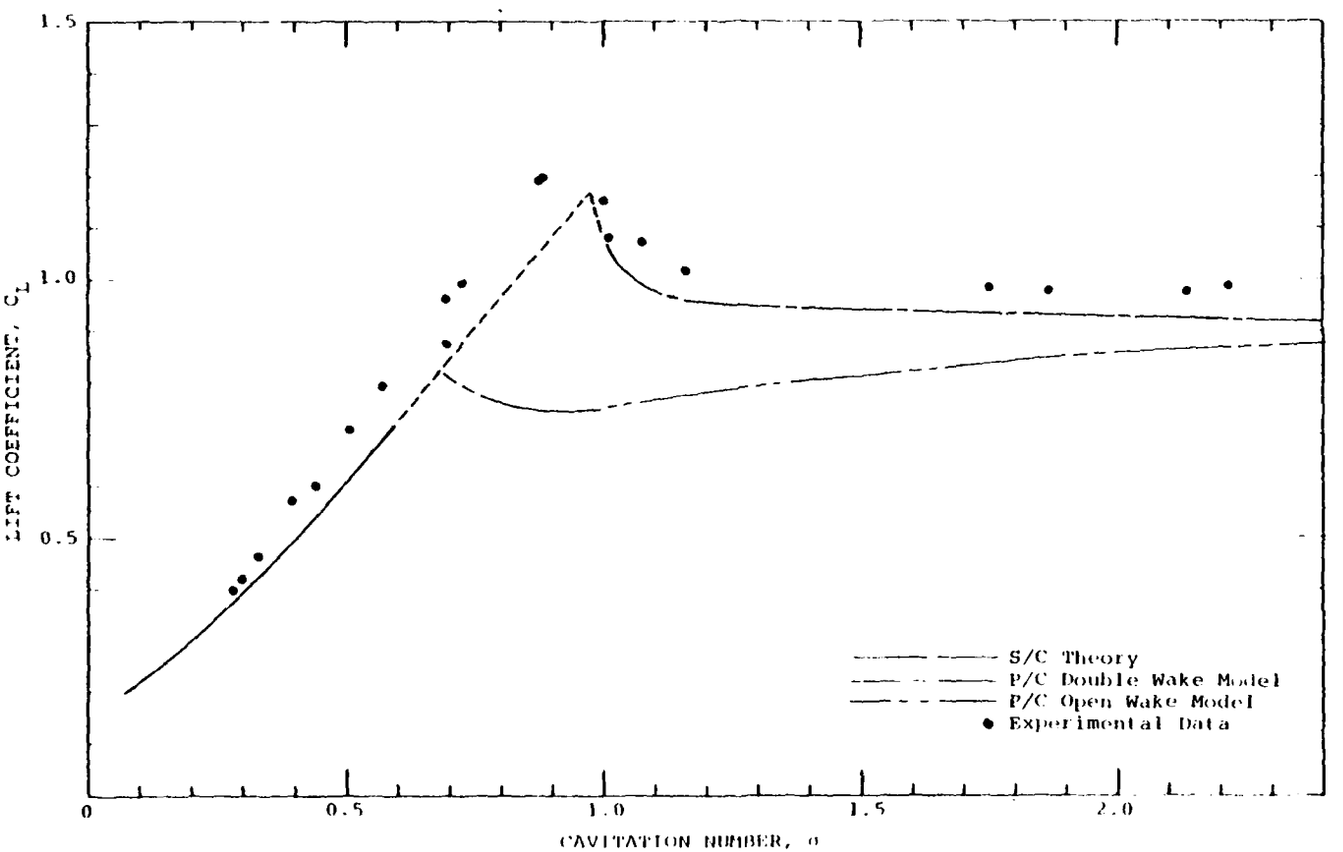

(d) $\alpha = 6°$

FIGURE 4.6 CONTINUED

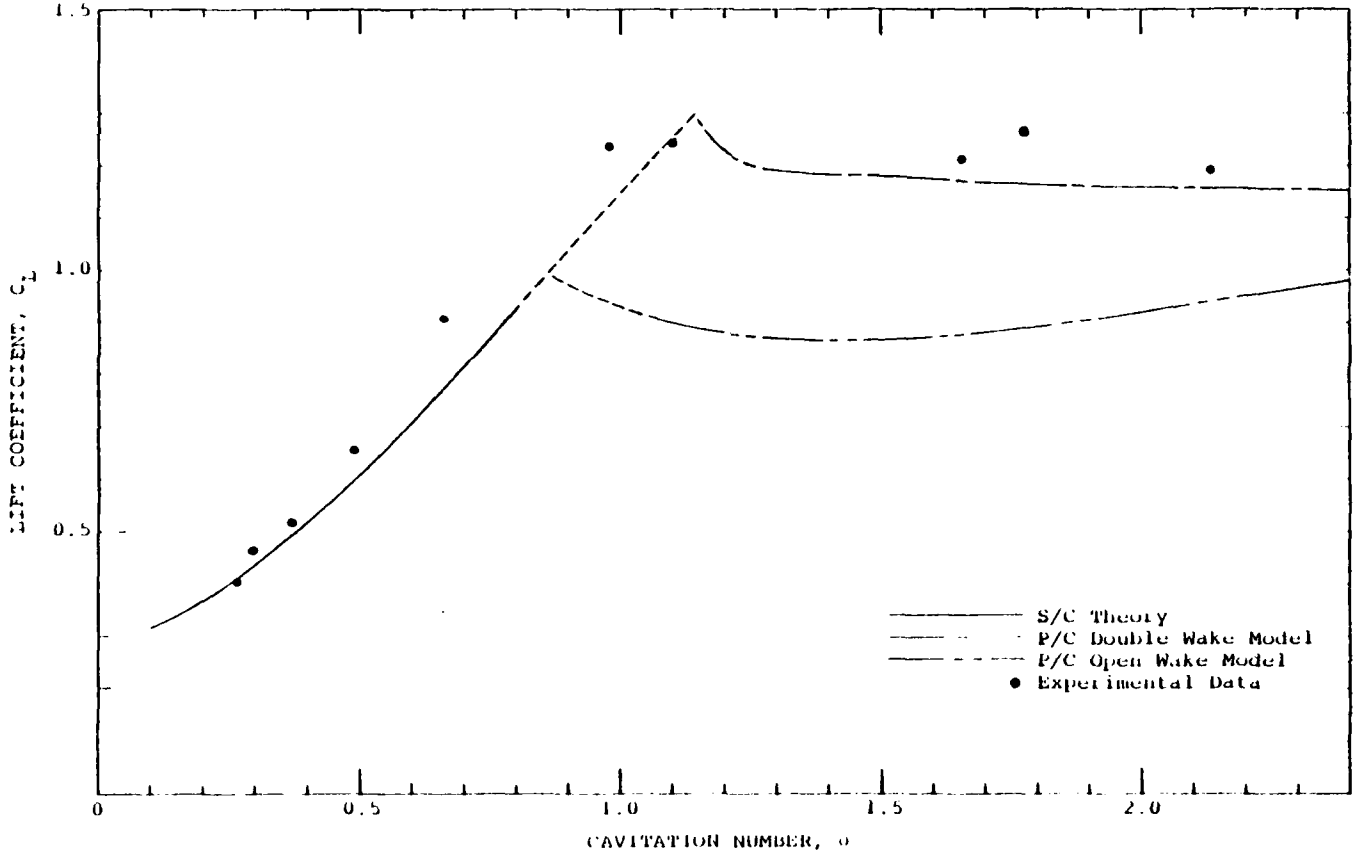

(e) α = 8°

FIGURE 4.6 CONTINUED

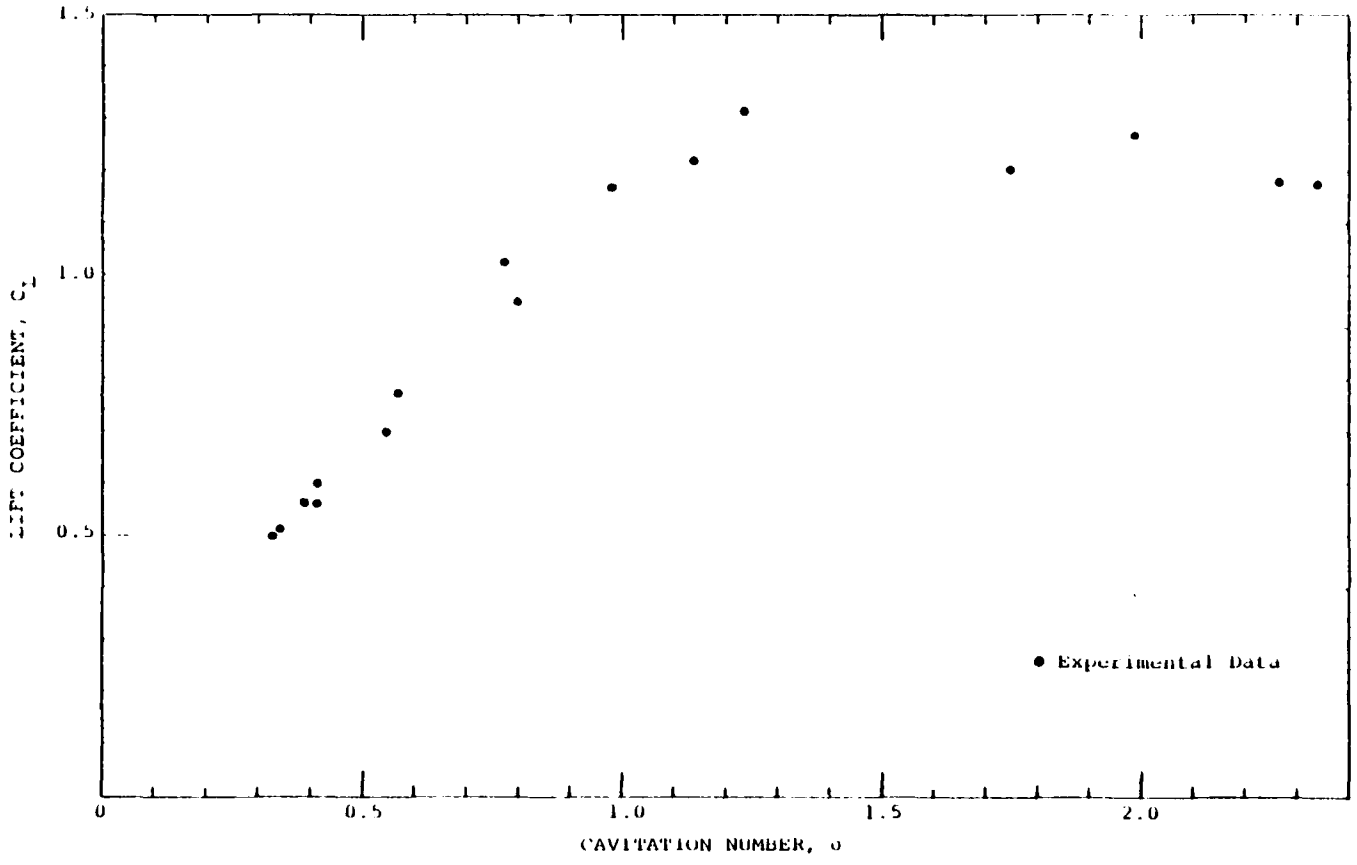

(f) $\alpha = 10°$

FIGURE 4.6 CONTINUED

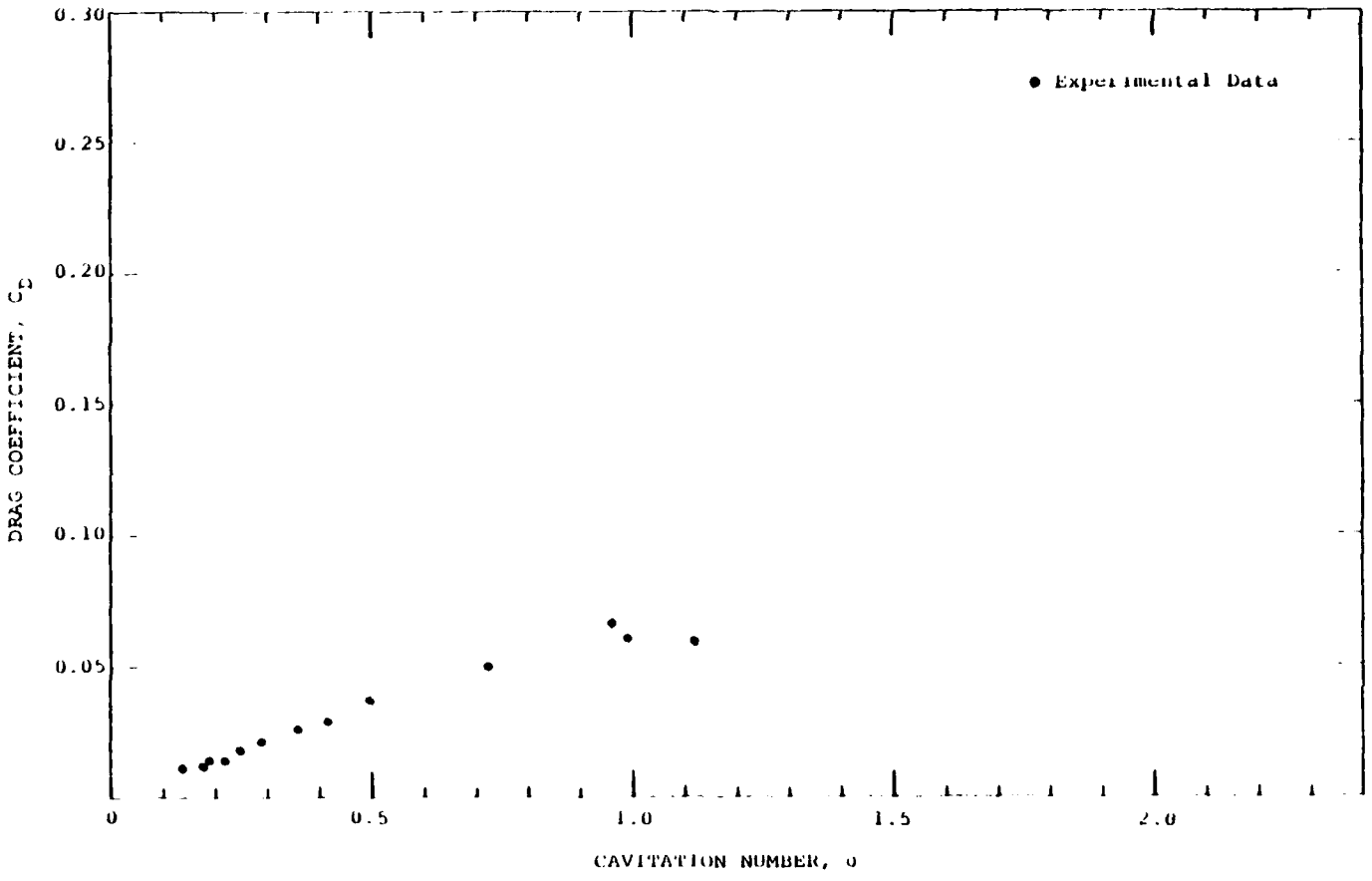

(a) $\alpha = 0°$

FIGURE 4.7
DRAG COEFFICIENT AS A FUNCTION OF CAVITATION NUMBER

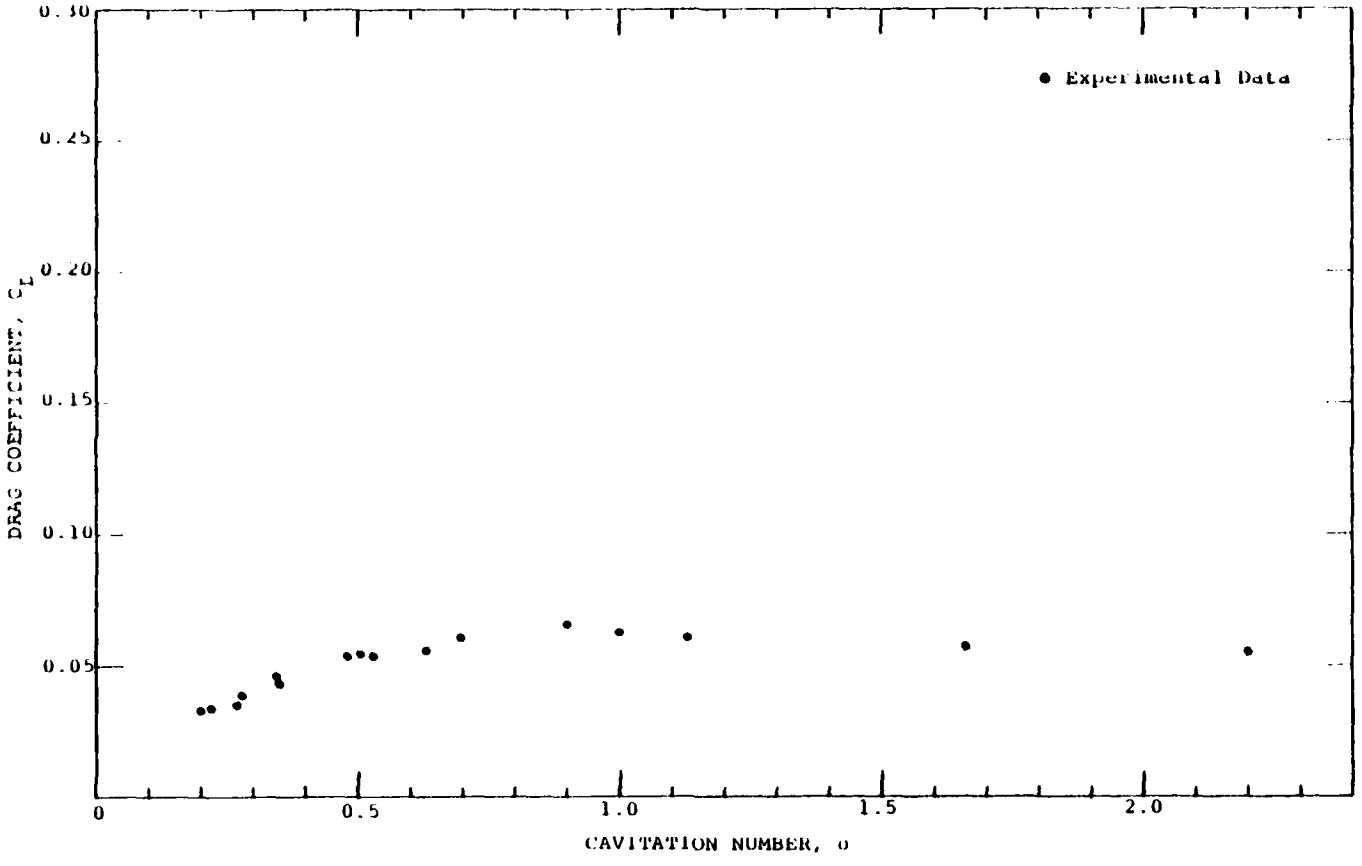

(b) $\alpha = 2°$

FIGURE 4.7 CONTINUED

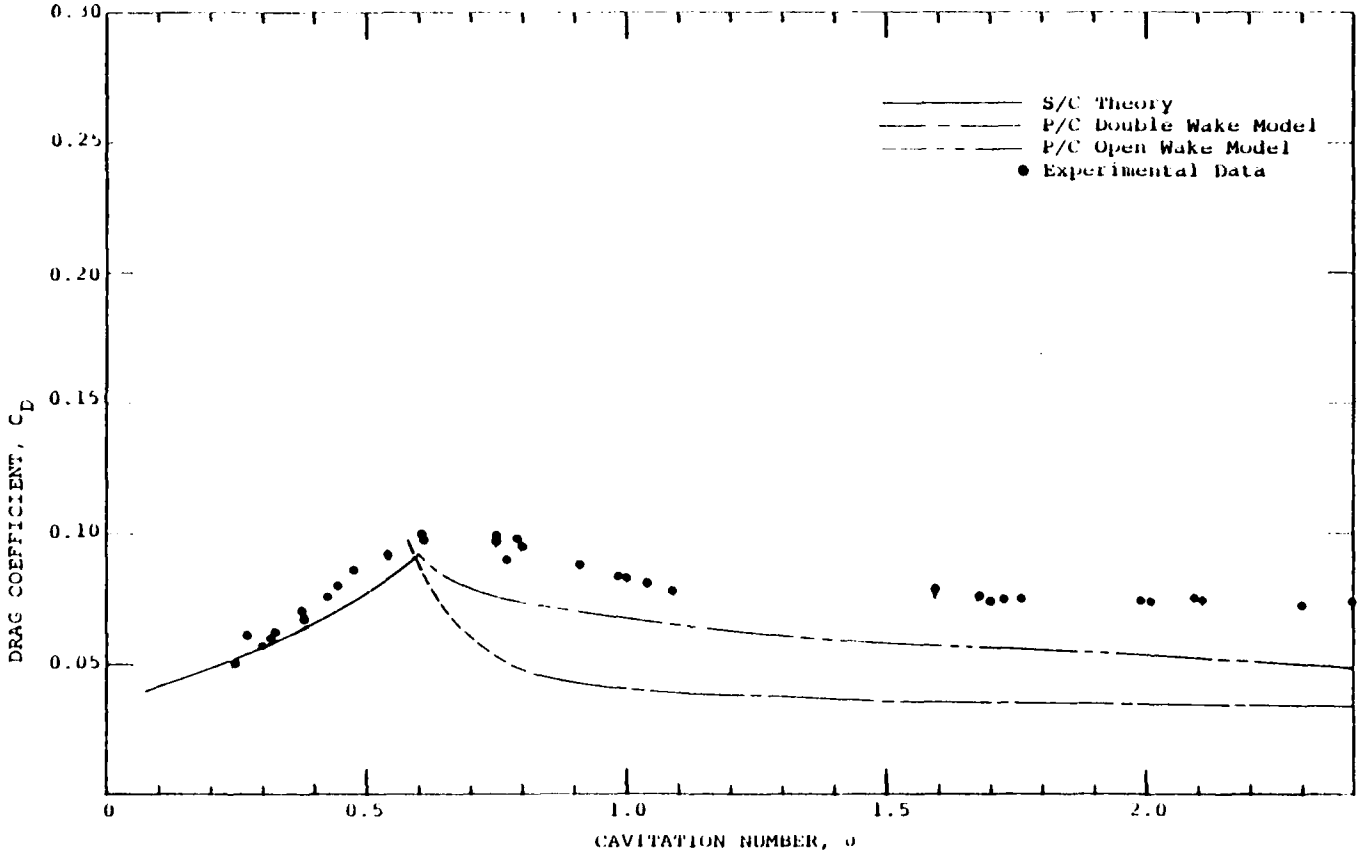

(c) $\alpha = 4°$

FIGURE 4.7 CONTINUED

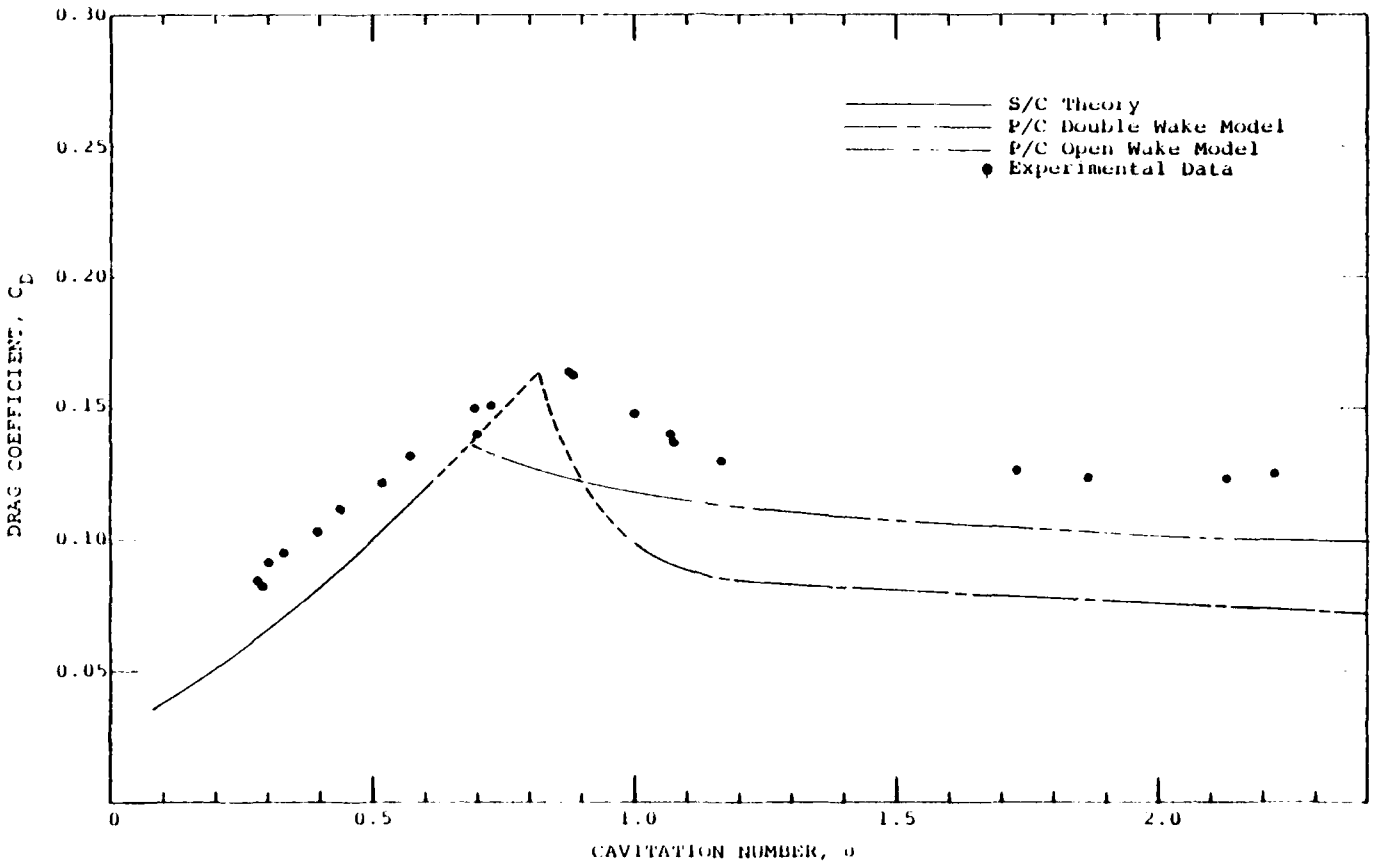

(d) $\alpha = 6°$

FIGURE 4.7 CONTINUED

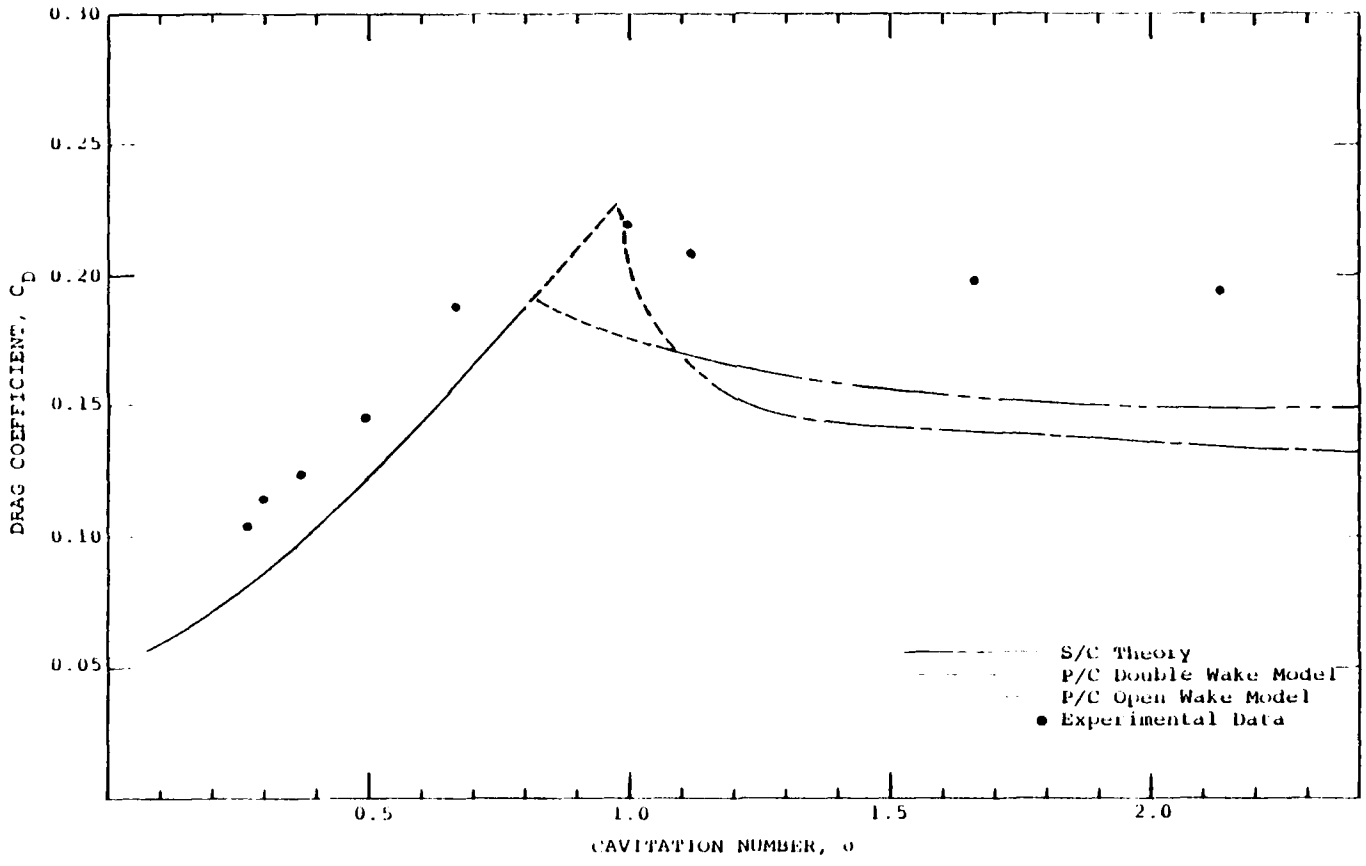

(e) $\alpha = 8°$

FIGURE 4.7 CONTINUED

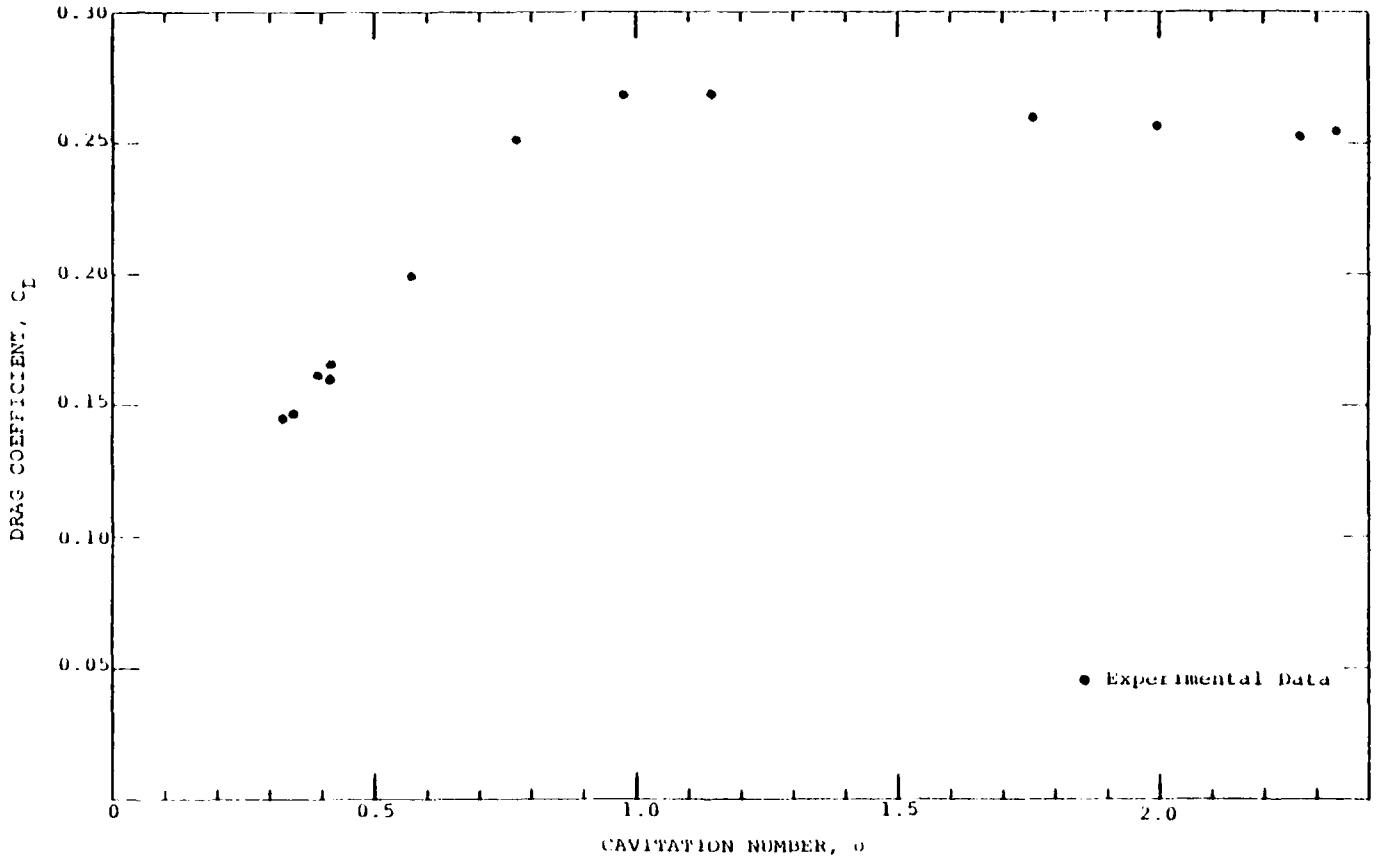

(e) $\alpha = 10°$

FIGURE 4.7 CONTINUED

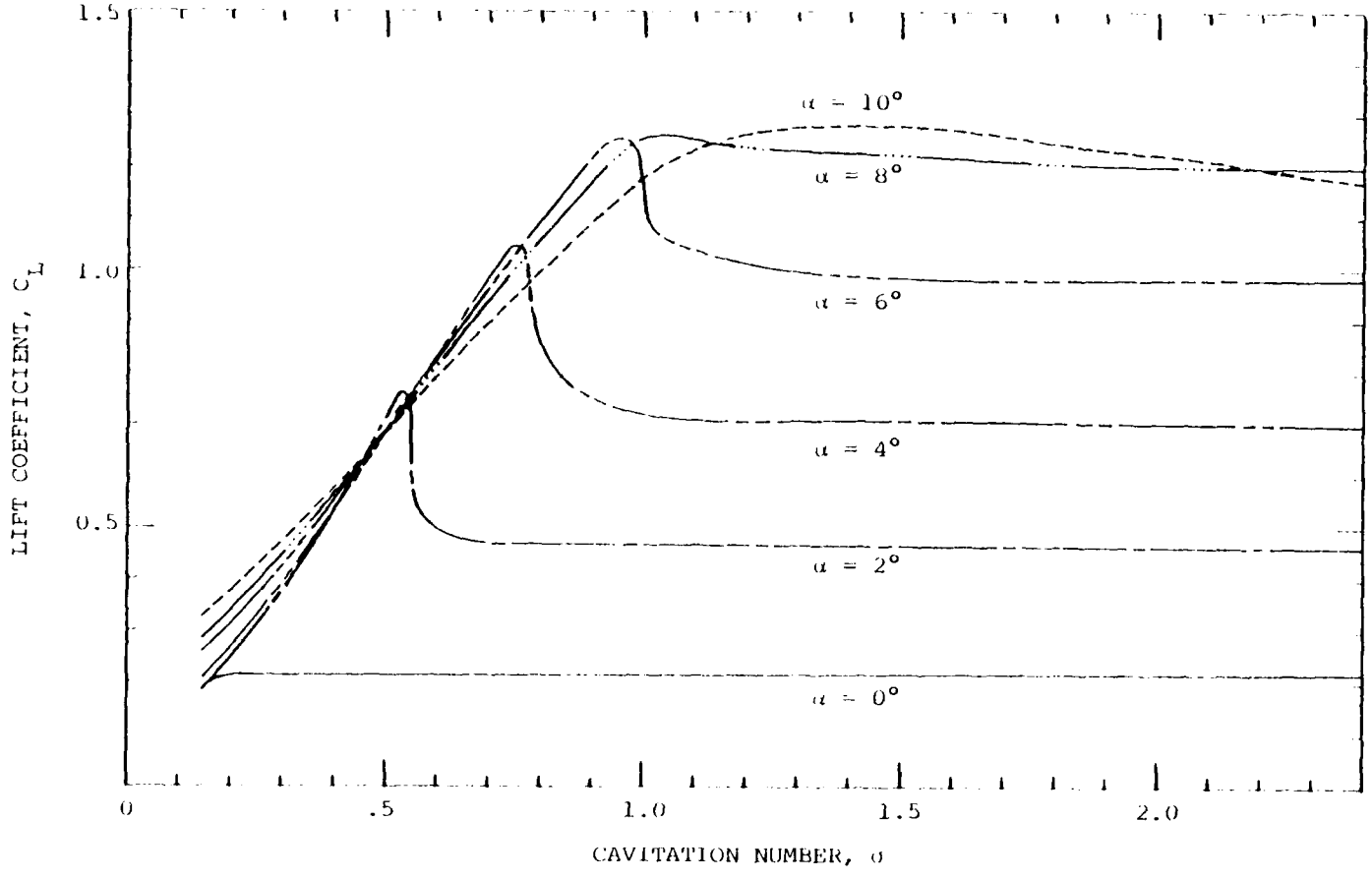

FIGURE 4.8
DRAG COEFFICIENT AS A FUNCTION OF CAVITATION NUMBER AND ANGLE OF INCIDENCE
(SUMMARY OF EXPERIMENTAL DATA)

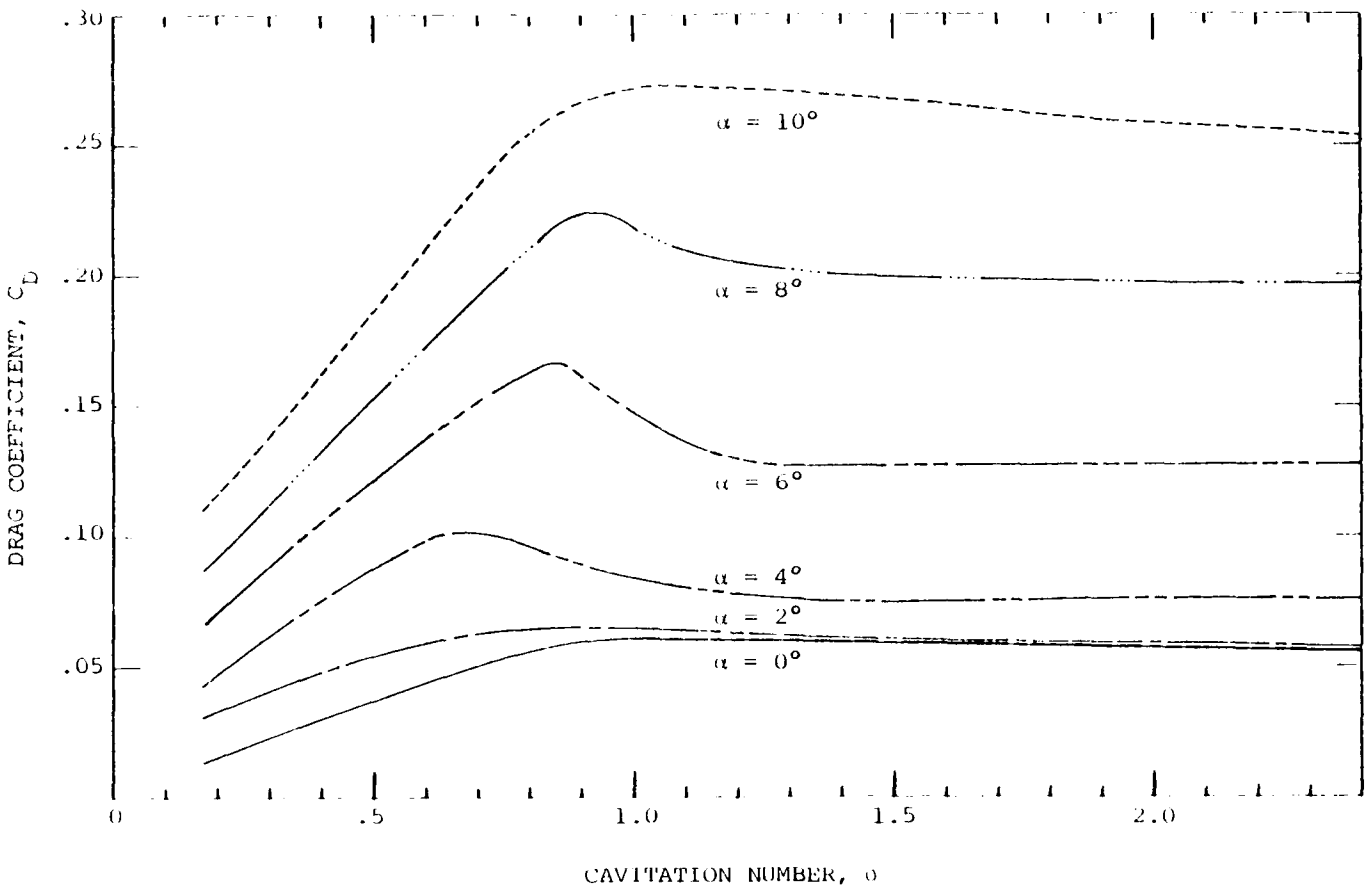

FIGURE 4.9
DRAG COEFFICIENT AS A FUNCTION OF CAVITATION NUMBER AND ANGLE OF INCIDENCE
(SUMMARY OF EXPERIMENTAL DATA)

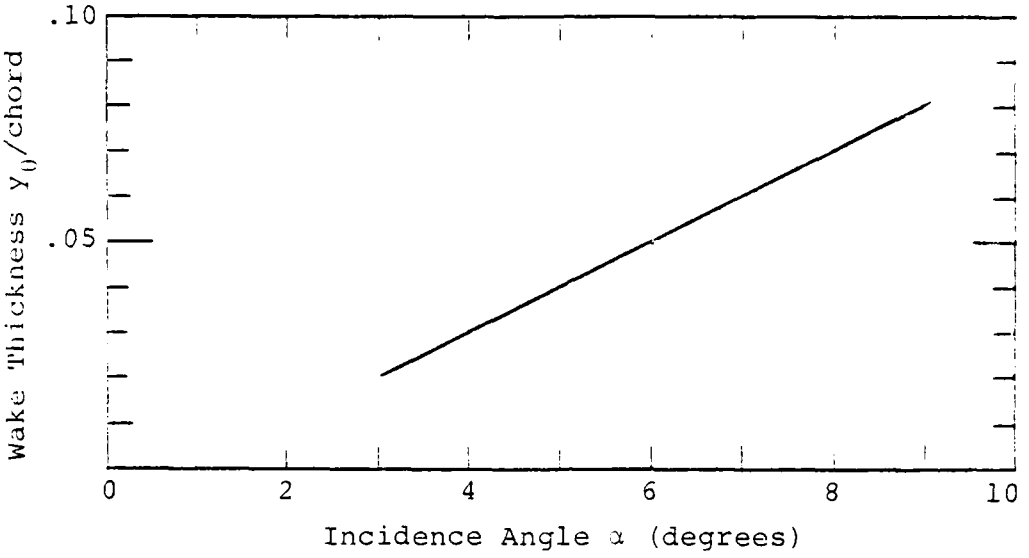

FIGURE 4.10
WAKE THICKNESS y_0 IN EQUATION (3.31)
USED FOR THE INFINITE WAKE MODEL
AT $\ell_c/c = 0.5$ WITH A
PROPORTIONALITY LAW FOR CHANGE OF ℓ_c

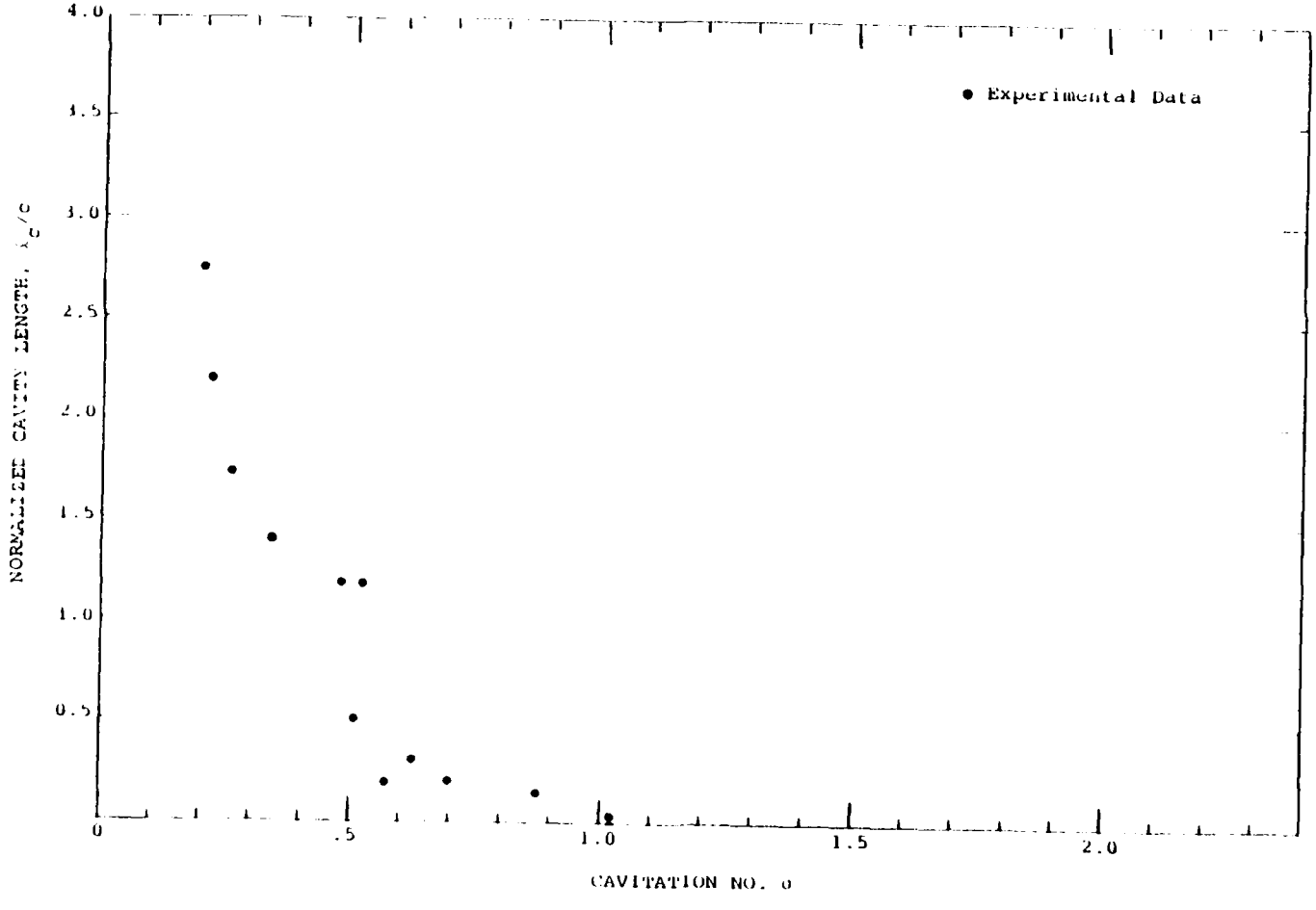

(a) $\alpha = 2°$

FIGURE 4.11
CAVITY LENGTH vs. CAVITATIO . NUMBER

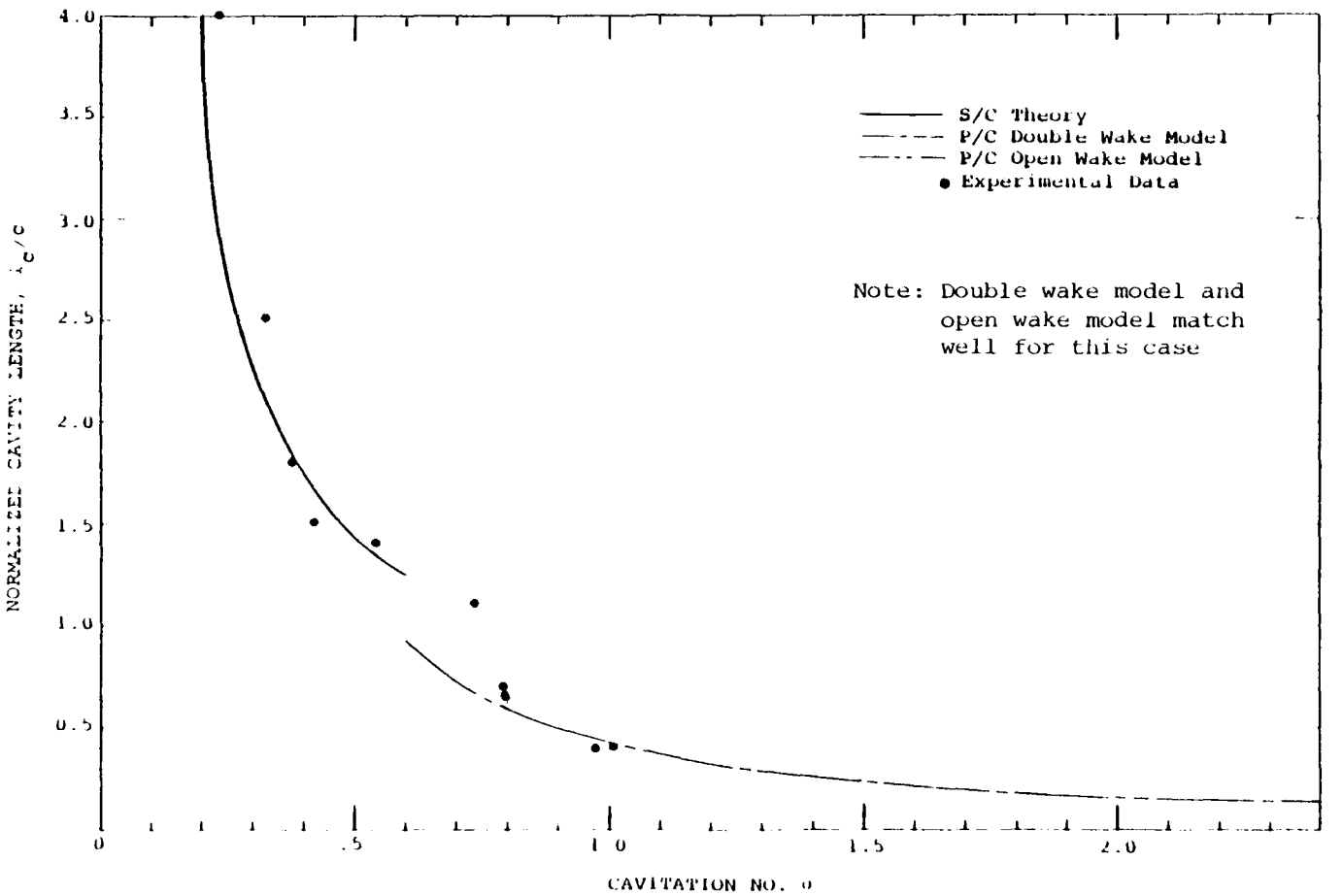

(b) $\alpha = 4°$

FIGURE 4.11 CONTINUED

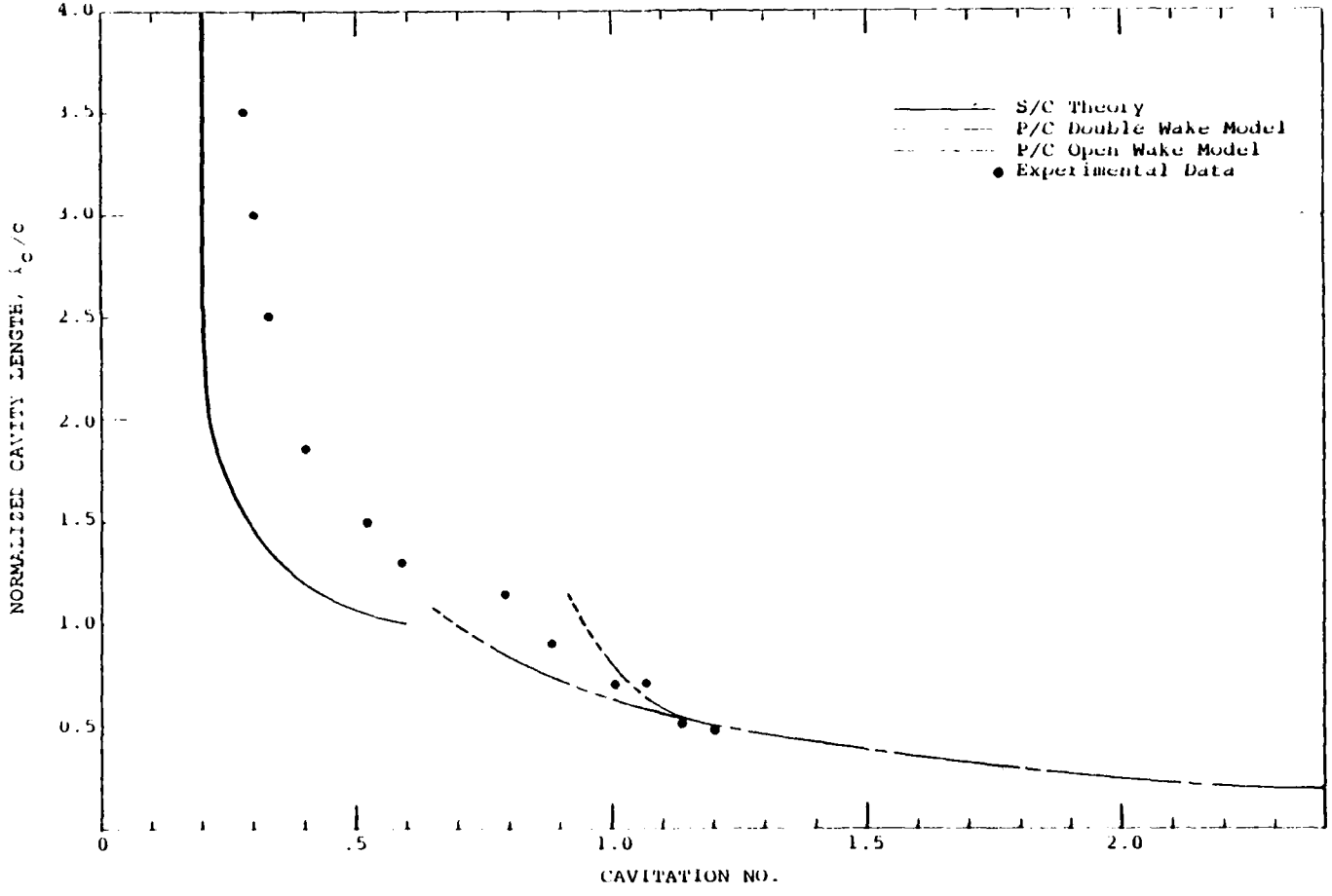

(c) $\alpha = 6°$

FIGURE 4.11 CONTINUED

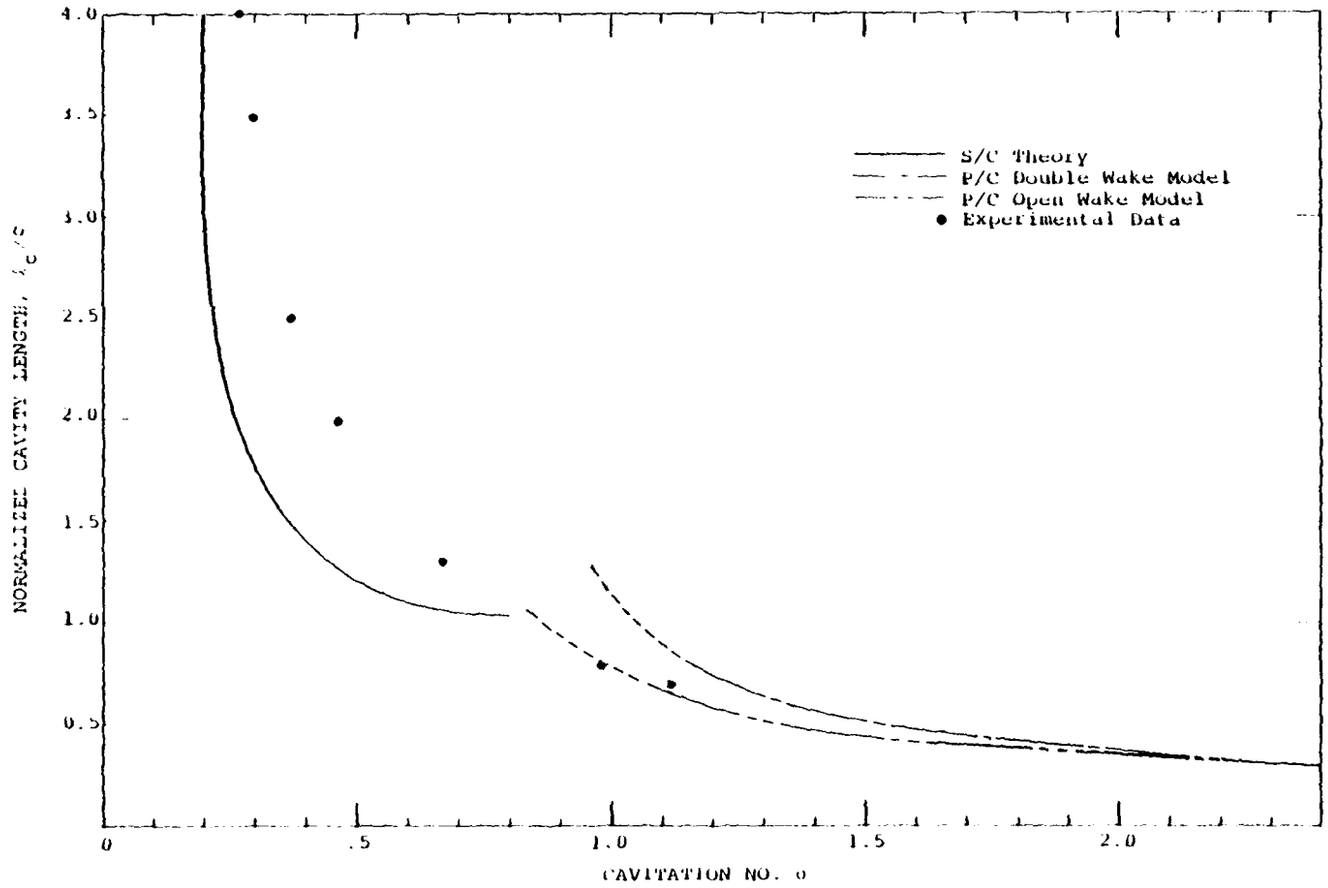

(d) $\alpha = 8°$

FIGURE 4.11 CONTINUED

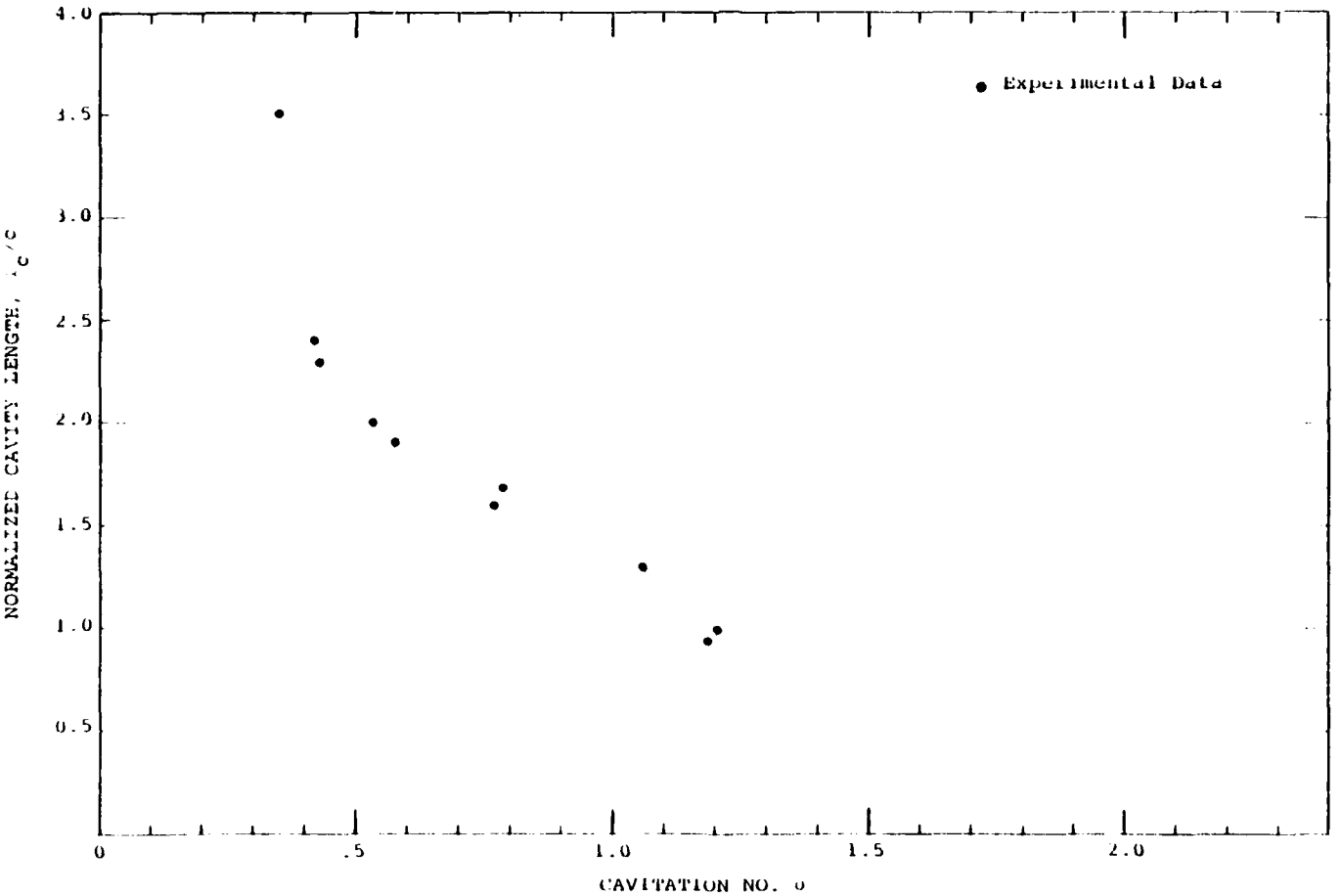

(e) $\alpha = 10°$

FIGURE 4.11 CONTINUED


DA
FILM